

Dielectric response of electrons with strong local correlations and long-ranged Coulomb interactions

B Sriram Shastry* and Michael Arciniaga

Physics Department, University of California, Santa Cruz, CA, 95064

March 19, 2023

Abstract

Motivated by recent experiments, we append long ranged Coulomb interactions to dominant strong local correlations and study the resulting t - J - V_C model for the 2-dimensional cuprate materials. This model includes the effect of short ranged Hubbard-Gutzwiller-Kanamori type correlations and long ranged Coulomb interactions on tight binding electrons. We calculate the $\{\vec{q}, \omega\}$ dependent charge density fluctuations in this model using the extremely correlated Fermi liquid theory characterized by quasiparticles with very small weight Z . We develop a novel set of formulae to represent the dynamical charge susceptibility and the dielectric function, using a version of the charge-current continuity equation for a band system valid for arbitrary \vec{q} . Combining these ingredients, we present results for the dynamical charge susceptibility $\tilde{\chi}_{\rho\rho}(\vec{q}, \omega)$, (longitudinal) dielectric function $\varepsilon(\vec{q}, \omega)$, current susceptibility $\tilde{\chi}_{JJ}(\vec{q}, \omega)$, conductivity $\sigma(\vec{q}, \omega)$, and the plasma frequency for any \vec{q} . We also present calculations for the first moment of the structure function and discuss a characteristic energy scale $\Omega_p(\vec{q})$ which locates a peak in $\text{Im } \tilde{\chi}_{\rho\rho}(\vec{q}, \omega)$.

*sriram@physics.ucsc.edu

1 Introduction

The role of strong local correlations and their interplay with long ranged Coulomb interactions, is an important problem in condensed matter physics. In the context of the metal insulator (Mott-Hubbard) transition of a Hubbard-Gutzwiller-Kanamori type model of strong correlations with added long ranged Coulomb interactions, early work [1–3] emphasized that this combination of the two types of interactions, quite generally leads to a metal with poor screening. These works noted that strong local correlations enhance the effective mass of electrons near a Mott transition, with $m^*/m \sim 1/(1 - U/U_c)$ at half filling $n = 1$, or with $m^*/m \sim \frac{1}{(1-n)}$ with $U \gg t$ [4] and U_c is the putative critical interaction strength discussed in [2]. These result in the enhancement of the density of states $\frac{dN}{d\mu} \propto \frac{m^*}{m}$, which in turn suppresses the screening constant q_s related by the compressibility sum-rule [5] (see Eq. (E.5, E.3, E.4) below):

$$q_s^2 = \frac{4\pi q_e^2}{a_0^3 N_s} \frac{dN}{d\mu} \rightarrow 0, \quad (1)$$

thereby increasing the screening length $\lambda_s = 2\pi/q_s$. More recent theoretical work [11, 12] has focussed on the dynamical aspects of screening, within the program of unifying band structure methods with dynamically screened Coulomb interaction and short ranged correlations. The latter are usually treated within the dynamical mean field theory [11, 12].

An immediate motivation for the present work comes from a set of experiments using the recently developed tool of momentum resolved electron energy loss spectroscopy (M-EELS) [13–15]. This technique gives a direct readout of the structure function $S(\vec{q}, \omega)$ or equivalently the dielectric function $\varepsilon(\vec{q}, \omega)$, for a broad range of momentum transfer \vec{q} and energy transfer ω . The initial application of this technique has provided high resolution data on the structure function for the archetypical strongly correlated cuprate superconducting material $Bi_{2.5}Sr_{1.9}CaCu_2O_{8+x}$ (BSSCO), for two samples with $T_c = 91K$ and $T_c = 50K$ respectively. In the normal state, the data looks very different from what one might expect for a conventional weakly correlated Fermi liquid, e.g., one describable by the random-phase approximation (RPA). Sharp features arising from long lived quasiparticles in that theory are rounded off to broad peaks, and the spectrum has surprisingly long frequency tails. Understanding the data seems to require reducing the quasiparticle domination in charge response functions, as argued in Ref. [16, 17].

In this work we extend the *extremely correlated Fermi liquid theory* (ECFL) [18], by adding the long ranged component of the Coulomb interaction. We thus calculate the charge dynamics of the t - J - V_C model Eq. (2), which is a generalization of the t - J model obtained by adding to it a long-ranged Coulomb interaction V_C . For this model we calculate the $\{\vec{q}, \omega\}$ dependent dielectric function $\varepsilon\{\vec{q}, \omega\}$ and the charge and current susceptibilities.

The ECFL theory was developed to describe the very large U Hubbard model, or equivalently the short ranged t - J interaction [18]. It therefore deals with the propagation and interaction of Gutzwiller projected electrons, obeying non-canonical anticommutators Eq. (8), within a tight binding model. The ECFL theory is characterized by a small but non-zero quasiparticle weight $Z \ll 1$ [18], and is therefore suitable for describing the above experiments.

The theory of the interacting 2-d electron system presented here differs significantly from earlier theories designed in the contexts of semiconductor inversion layers, surfaces of metals and more recently for graphene [22–25]. In the current study, the dominant interaction is the short ranged Coulomb repulsion on the scale of a single atom, i.e., the Gutzwiller-Hubbard correlation. If one starts from weakly-interacting electrons within a perturbative scheme, it is very difficult to build in the strong local correlations, since the perturbation parameter is the largest energy scale! We start instead with non-canonical Gutzwiller projected electrons $\tilde{C}_{i\sigma}$ Eq. (2, 8), and then introduce long ranged Coulomb interactions, giving the t - J - V_C model. In this treatment the physics of the Mott-Hubbard insulator at half filling is obtained naturally, in view of the inbuilt Gutzwiller projection. This generalized ECFL calculation provides a microscopic theory of charge fluctuations in a metal, with fragile quasiparticles. We provide results for sum-rules, plasma frequencies and other measurable quantities, as functions of a few model parameters.

1.1 Highlights of new formulas

The calculations on this t - J - V_C model use the *extremely correlated Fermi liquid* (ECFL) theory [18] for the t - J model. The highly correlated single electron Green’s function of this theory $\mathcal{G}(\vec{k}, \omega)$, has been calculated recently in a controlled expansion to $\mathcal{O}(\lambda^2)$ [20, 21]. This theory produces an electron liquid with a very small, but non-zero quasiparticle weight Z . It therefore has a fair *a-priori* possibility of

reproducing the broad backgrounds seen in experiments. We also note that the ECFL theory provides a quantitative set of results for resistivity of cuprates for the single layer compounds [31] in fair agreement with a large body of data. It also provides a set of results for the inelastic non-resonant Raman scattering in different channels for the t - J model from the fluctuations of the kinetic energy components [30], that give a fair account of Raman scattering experiments [34, 35].

In order to calculate the fluctuations of the charge density, one needs information beyond that contained in $\mathcal{G}(\vec{k}, \omega)$. We require the two particle response rather than the single particle Green's functions. Generalizing the ECFL calculations in that direction is a non-trivial task. Therefore we are obliged to make approximations using the correlated single particle Green's functions.

This work extends the general formalism in two important directions described in the next paragraph. These extensions enable the formulation of suitable approximations using the available Green's functions $\mathcal{G}(\vec{k}, \omega)$. We describe these two extensions, and record their location in this paper. Some readers might find these extensions of potential use in problems other than the one considered here. Other readers interested in the concrete applications made here, can use this roadmap to skip certain sections and appendices.

The first formal result is Eq. (50, 54). This formula is valid for any density response function that admits a high frequency moment expansion in powers of ω^2 Eq. (F.4, F.8). It expresses the $\{\vec{q}, \omega\}$ dependent irreducible susceptibility in terms of (i) its static limit, (ii) the leading high frequency moment and (iii) the complex self energy $\Psi(\vec{q}, \omega)$ for this object. This self energy $\Psi(\vec{q}, \omega)$ has not been discussed in literature, as far as we are aware. It is obtained following a Luttinger type analysis of the susceptibility [26], by reorganizing the moment expansion formulas.

The next formal result is the derivation of an important pair of alternate formulas Eq. (32, 43) for the dielectric function valid for all \vec{q}, ω . While Eq. (32) is a familiar expression in terms of the density operator, Eq. (43) is new and involves the W operator, which is the divergence of the lattice current operator as seen in Eq. (9, 10). These formulas are modeled after analogous formulas due to Nozières in Ref. [5], valid for the (continuum) homogeneous electron gas. In the latter context, Nozières uses diagrammatic perturbation theory and regroups terms so that the conservation of charge is reflected in the relationship between appropriate correlation functions- thus finally leading to his twin formulas.

The two alternate formulas Eq. (29, 28) for the *inverse* dielectric constant are relatively more straightforward, and follow from the continuity equation. These involve the reducible correlation functions $\chi_{\rho\rho}$, and provide the starting point for obtaining the Nozières type formulas, which are analogous relations for the *irreducible* susceptibility $\tilde{\chi}_{\rho\rho}$. The connection between the reducible i.e. $\chi_{\rho\rho}$, and irreducible i.e. $\tilde{\chi}_{\rho\rho}$ susceptibilities is straightforward when the electrons are canonical. The relationship is expressed using Feynman diagrams, which encode perturbation theory compactly and elegantly, as shown in text books [5, 10]. However for the t - J - V_C model, we are dealing with non-canonical electrons, and hence the identification and extraction of irreducible pieces needs to be accomplished without the use of vertex functions, or of manipulating sums of Feynman diagrams. The needed analysis is carried out in Section-(4). The method employed by us decomposes the charge source, i.e. an auxiliary external potential used to generate the Greens functions into a part containing a Hartree type term from the remainder as described in Section-(4) and Appendix-(C, D). As stated, this leads to the final formulas Eq. (32, 43), with a central result being the identity Eq. (39), relating the (irreducible) charge and W -type correlations functions. The W -type response functions involve the W -type vertex Eq. (10, 9), these contain the full set of hopping parameters in the tight binding model, and crucially for our purposes, enable us to address the \vec{q}, ω dependence of the charge response over the *entire* Brillouin zone. It is also evident that by taking the long wavelength limit $\lim_{q \rightarrow 0}$, we recover the homogeneous electron gas relations originally written by Nozières [5].

Combining the formal expressions Eq. (50, 54) for the charge and W -type susceptibilities with the twin Nozières type relations Eq. (32, 43) enables us to make useful approximations for the charge response. We use the ECFL single particle Green's functions \mathcal{G} to perform the explicit calculations, and thereby obtain two independent bubble susceptibilities Eq. (61, 62). These are the basic computations from ECFL. Using them in Eq. (64, 65), we get two alternate estimates of the irreducible charge susceptibility $\tilde{\chi}_{\rho\rho}(\vec{q}, \omega)$, and there from the dielectric constant by using Eq. (32). If we were to use exact (instead of bubble) susceptibilities, these two results would coincide, by virtue of the exact result Eq. (39). Since the approximations for the bubble calculations are not exact, these two estimates differ from each other in general. In fact these provide two complementary approximations, valid in different regimes $\omega \rightarrow 0$ and $|\omega| \gg t$ (t is the hopping parameter). We then combine expressions Eq. (50, 54), guided by considerations of validity at low and high ω as summarized in Appendix-(F) and Appendix-(E). We finally arrive at alternate approximations Eq. (69, 70). These two approximations are overall similar in most features.

They only differ at very small \vec{q}, ω where quasiparticle excitations that are missing in Eq. (69), but are present in Eq. (70), cause some differences. Another novel result presented here is the identification of an important characteristic energy scale $\Omega_p(\vec{q})$. This scale locates a peak in $\text{Im} \tilde{\chi}_{\rho\rho}(\vec{q}, \omega)$ Eq. (56, 59), and is also expressible as a specific moment of the $\text{Im} \tilde{\chi}_{\rho\rho}(\vec{q}, \omega)$ in Eq. (80, F.20). We present results for this scale and show that it is quite low at small \vec{q} .

1.2 The plan of the paper

We define the t - J - V_C model below in Section-(2), and summarize the method used to calculate the charge response. The calculation uses the ECFL theory to calculate the electron Green's function \mathcal{G} to a certain approximation (termed as $\mathcal{O}(\lambda^2)$), which has been described in detail in our recent publications [20, 21]. To make this work self contained, we summarize the scheme and the equations used to compute \mathcal{G} in Appendix-(A).

In Appendix-(B) we recall the formal definitions of the susceptibility and the structure function for describing the charge response. Section-(3) summarizes the definitions of charge $\chi_{\rho\rho}$ and “current-type” susceptibilities χ_{WW} , and their cross susceptibilities $\chi_{\rho W}, \chi_{W\rho}$, for electrons in a narrow band, and their mutual relationship from the conservation law of charge.

In Appendix-(C) we define the electronic Green's function \mathcal{G} , its equation of motion generated conveniently by external potentials, which include a charge and a current source, and express the susceptibilities in terms of variational derivatives of the Green's functions, with respect to the external potentials.

Instead we present the necessary formal results here, directly using the susceptibilities. The strategy used is to redefine the external potential by absorbing a Hartree type term into it, as described in Appendix-(D).

We define in Appendix-(D) the irreducible susceptibilities $\tilde{\chi}_{\mu\nu}$ in terms of the reducible ones. The irreducible susceptibilities are calculated by taking functional derivatives of the Green's function \mathcal{G} . The details of the formalism are provided in Appendix-(D). The dielectric function satisfies a *linear* relationship Eq. (32) with it, in contrast to the non-linear relation with the reducible susceptibility Eq. (29). In Appendix-(D) we show that the conservation laws connect the screened, or irreducible susceptibilities with results that parallel those for canonical electrons.

In Section-(4) we express the susceptibilities in terms of their screened, or irreducible pieces $\tilde{\chi}_{\rho,\rho}, \tilde{\chi}_{\rho,W}, \tilde{\chi}_{W,\rho}, \tilde{\chi}_{W,W}$. We find a useful and important pair of formulas Eq. (32, 43). These relations, obtained for tight-binding non-canonical electrons, are completely analogous to the results of Ref. [5], who worked with canonical electrons in the continuum, i.e., for the homogeneous electron gas. In these exact formulas, the dielectric function at arbitrary (\vec{q}, ω) is expressed in alternate forms involving two different pairs of correlation functions. These alternate forms work better in complementary regions of ω and allow us to make useful approximations, as explored in Appendix-(E.1) and in Appendix-(E.2).

The frequency sum-rules for the susceptibility play an important role in our theory and are summarized in Appendix-(F). The limiting values of the dielectric constant at low and high ω are noted in Appendix-(E).

In Section-(5) the formulae that approximates the dielectric function is presented and applications of the methodology to the computation of the dielectric function is described. In Section-(6) we discuss the results and present some conclusions.

2 The t - J - V_C model

The t - J - V_C Hamiltonian studied here is

$$H = H_t + H_J + V_C \quad (2)$$

$$H_t = - \sum_{ij\sigma} t_{ij} \tilde{C}_{i\sigma}^\dagger \tilde{C}_{j\sigma} - \mu \sum_i n_i \quad (3)$$

$$H_J = \frac{1}{2} \sum_{ij} J_{ij} (\vec{S}_i \cdot \vec{S}_j - \frac{n_i n_j}{4}) \quad (4)$$

$$V_C = \frac{1}{2} \sum_{i \neq j} V_{ij} n_i n_j, \quad V_{ij} = \frac{1}{\epsilon_\infty} \frac{q_e^2}{|\vec{r}_i - \vec{r}_j|} \quad (5)$$

with the electronic charge $q_e = -|e|$, the density operator $n_i = \sum_\sigma \tilde{C}_{i\sigma}^\dagger \tilde{C}_{i\sigma}$, and spin density operator $S_i^\alpha = \frac{1}{2} \sum_{\sigma\sigma'} \tilde{C}_{i\sigma}^\dagger \tau_{\sigma\sigma'}^\alpha \tilde{C}_{i\sigma'}$, τ^α is a Pauli matrix, and the Coulomb potential is denoted by V_{ij} . The

hopping parameters $-t_{ij} = \frac{1}{N_s} \sum_{ij} e^{i\vec{k}(\vec{r}_i - \vec{r}_j)} \varepsilon_k$ are Fourier components of the band energy ε_k , N_s is the number of sites in the crystal. We will study both 3 and 2 dimensional (layered) strongly correlated electron systems, where the Fourier components of V is given in 3-d, assuming a simple cubic cell of side a_0 by

$$V(\vec{q}) = \frac{1}{N_s a_0^3 \varepsilon_\infty} \frac{4\pi q_e^2}{|\vec{q}|^2} \quad (3\text{-d}), \quad (6)$$

and in 2-d by

$$V(\vec{q}) = \frac{1}{N_s a_0^2 \varepsilon_\infty} \frac{2\pi q_e^2}{|\vec{q}|} \quad (2\text{-d}). \quad (7)$$

To simplify notation we will set $\hbar = 1$ and the lattice constant $a_0 = 1$ in most part below. Here ε_∞ is the static dielectric constant due to screening by mobile charges other than the ones described by H_t , if any are present. Here the correlated Fermi destruction operator \tilde{C}_i is found from the plain (i.e. canonical or unprojected) operators c_i , by sandwiching it between two Gutzwiller projection operators $\tilde{C}_{i\sigma} = P_G C_{i\sigma} P_G$. Let us note that these Fermions satisfy a non-canonical set of anticommutation relations

$$\begin{aligned} \{\tilde{C}_{i\sigma_i}, \tilde{C}_{j\sigma_j}^\dagger\} &= \delta_{ij} \left(\delta_{\sigma_i \sigma_j} - \sigma_i \sigma_j \tilde{C}_{i\bar{\sigma}_i}^\dagger \tilde{C}_{i\bar{\sigma}_j} \right), \text{ and} \\ \{\tilde{C}_{i\sigma_i}, \tilde{C}_{j\sigma_j}\} &= 0. \end{aligned} \quad (8)$$

The physical meaning of this sandwiching process is that the Fermi operators act within the subspace where projector P_G enforces single occupancy at each site. This model generalizes the well studied t - J model by adding the long ranged Coulomb interaction term, and we will study the effect of the added term in determining the fluctuations of the charge density, the dielectric function and related structure function. We initially keep the dimensionality of the electronic system general so that the results apply to 3-dimensions, and later consider the case of 2-dimensional stacking of the electronic system, for modeling cuprate superconductors.

The t - J - V_C model used here neglects multi-band aspects of the Coulomb interaction, and focusses on the extremely correlated single band containing the Fermi surface. It throws out inter-band transition matrix elements of the Coulomb interaction and only retains intraband terms. A rough account of the other bands is taken, by rescaling the Coulomb interaction by an infinite frequency dielectric constant ε_∞ as in Eq. (5). This rescaling represents the cumulative effect of the ‘fast’ (i.e. high energy) electrons on the ‘slow’ (low energy) correlated electrons described by our model. This type of reasoning suggests that as long as the excitation energies do not exceed the inter-band energies, the single band model employed here should be quite reliable.

In applying the results of these calculations to real systems, it must be kept in mind that the t - J - V_C model is only a ‘low energy’ abstraction of the narrow band containing the Fermi energy, which is further embedded in a continuum of bands extending to very high energies. Thus, in an experimental situation, curtailing the frequency integration in Eq. (F.4) up to a cutoff frequency $\Omega \sim 1, 2$ eV is expected to capture the ‘low energy’ model, with strong correlations built into the results. On the other hand by extending the integral to higher energies, one gets rid of the correlations and the results should reveal the bare electron scales.

3 Reducible susceptibilities and Conservation laws

In this section we outline the relationship between two reducible (dynamical) susceptibilities $\chi_{\rho\rho}$ and χ_{WW} for interacting electrons on a lattice, which follows from the conservation of charge. The basic definition of the susceptibility χ_{AB} for any pair of operators is given in Eq. (B.1, B.8), the local operators $\rho_m = q_e \sum_\sigma \tilde{C}_{m\sigma}^\dagger \tilde{C}_{m\sigma}$ correspond to the charge density of electrons at site m and W to the divergence of the lattice current defined in Eq. (9, 10) below. These susceptibilities and their easily derived relationship is valid at all (\vec{q}, ω) , and is then generalized to an almost identical relationship between irreducible susceptibilities below. This generalization is technically non-trivial, and is one of the main formal results of this work. Since it is likely to be of interest to specialists, we have separated out the derivation to appendices, and keep the main text relatively free of these details.

The charge conservation laws follow from the basic observation that both H_J and V_C in the Hamiltonian commute with the local charge density ρ_m , thereby only H_t governs its equation of motion. We

find the commutator of ρ_m can be expressed by an exact relation involving a Hermitian operator W_m

$$[H, \rho_m] = -iW_m, \text{ where } W_m = iq_e \sum_{n\sigma} t_{mn} \left(\tilde{C}_{m\sigma}^\dagger \tilde{C}_{n\sigma} - \tilde{C}_{n\sigma}^\dagger \tilde{C}_{m\sigma} \right). \quad (9)$$

Defining its Fourier component W_q through

$$\begin{aligned} W_m &= \frac{1}{N_s} \sum_q e^{i\vec{q} \cdot \vec{r}_m} W_{\vec{q}}, \\ W_{\vec{q}} &= iq_e \sum_{k\sigma} (\varepsilon_{\vec{k}} - \varepsilon_{\vec{k}+\vec{q}}) \tilde{C}_{k\sigma}^\dagger \tilde{C}_{\vec{k}+\vec{q}\sigma}, \quad W_{\vec{q}}^\dagger = W_{-\vec{q}}, \end{aligned} \quad (10)$$

the conservation law for charge can be rewritten as

$$[H, \rho_{\vec{q}}] = -iW_{\vec{q}}. \quad (11)$$

We may think of the W -variable as the lattice counterpart of the divergence of the current $\vec{\nabla} \cdot \vec{J}$ from the following considerations. While Eq. (11) is valid for arbitrary q , in the long wavelength limit $q \rightarrow 0$, we note that

$$\lim_{q \rightarrow 0} W_q \rightarrow -i\vec{q} \cdot \vec{J}_{\vec{q}}, \quad (12)$$

where the electrical current operator $\vec{J}_{\vec{q}} = q_e \sum_{k\sigma} \left(\vec{\nabla} \varepsilon_k \right) \tilde{C}_{k\sigma}^\dagger \tilde{C}_{\vec{k}+\vec{q}\sigma}$. Hence Eq. (11) becomes the familiar continuity equation

$$\left([H, \rho_{\vec{q}}] + \vec{q} \cdot \vec{J}_{\vec{q}} \right) \big|_{q \rightarrow 0} = 0 \quad (13)$$

With this remark it is clear that Eq. (11) can be taken as the condition for conservation of charge at arbitrary wavelengths.

This leads us to consider in addition to the charge susceptibility, the three W -susceptibilities

$$\begin{aligned} \chi_{WW}(\vec{q}, \tau) &\equiv \chi_{W_{\vec{q}}W_{-\vec{q}}}(\tau); \\ \chi_{\rho W}(\vec{q}, \tau) &\equiv \chi_{\rho_{\vec{q}}W_{-\vec{q}}}(\tau); \\ \chi_{W\rho}(\vec{q}, \tau) &\equiv \chi_{W_{\vec{q}}\rho_{-\vec{q}}}(\tau). \end{aligned} \quad (14)$$

Note here that the location of W in the subscript determines the sign of the attached wave vector.

For completeness we note that the optical conductivity is written in terms of a current-susceptibility (see Eq. (E.15)). The unscreened current-current susceptibility can be written in the same fashion as Eq. (14)

$$\chi_{JJ}(\vec{q}, \tau) \equiv \chi_{J_q J_{-q}}(\tau). \quad (15)$$

Using Eq. (12) we can relate this to χ_{WW} for small \vec{q}

$$\text{For } |\vec{q}|a_0 \ll 1, \quad \chi_{WW}(\vec{q}, \tau) \rightarrow |\vec{q}|^2 \chi_{JJ}(\vec{q}, \tau). \quad (16)$$

The screened current-current susceptibility satisfies an analogous relation discussed later in Eq. (E.14).

In Eq. (C.13) and related equations we use the same symbol to represent the real space versions of the susceptibilities. It should be straightforward to distinguish between the two usages from their contexts. Let us first note the relationships between these and the charge susceptibility. From Eq. (B.8) we note that $\chi_{\rho\rho}(\vec{q}, \tau) = \langle T_\tau \rho_{\vec{q}}(\tau) \rho_{-\vec{q}}(0) \rangle$ and therefore on taking successive τ -derivatives we get

$$\frac{d}{d\tau} \chi_{\rho\rho}(\vec{q}, \tau) = (-i) \chi_{W\rho}(\vec{q}, \tau) \quad (17)$$

where we used the vanishing of the equal time commutator $[\rho_q, \rho_{-q}]$. Taking a further derivative we find

$$\begin{aligned} \frac{d}{d\tau} \chi_{W\rho}(\vec{q}, \tau) &= \delta(\tau) \langle [W_{\vec{q}}, \rho_{-\vec{q}}] \rangle - \chi_{W[H, \rho]}(\vec{q}, \tau) \\ &= -iN_s \kappa(\vec{q}) \delta(\tau) + i \chi_{WW}(\vec{q}, \tau), \end{aligned} \quad (18)$$

and taking \vec{q} along the x axis

$$\kappa(\vec{q}) = \frac{2q_e^2}{N_s} \sum_{k\sigma} \left(\varepsilon_{\vec{k}+\vec{q}} - \varepsilon_{\vec{k}} \right) \langle \tilde{C}_{\vec{k}\sigma}^\dagger \tilde{C}_{\vec{k}\sigma} \rangle. \quad (19)$$

For general non-parabolic bands

$$\lim_{q \rightarrow 0} \kappa(\vec{q}) = |\vec{q}|^2 \mathcal{T} \quad (20)$$

where the variable \mathcal{T} (equal to the stress tensor per site $\frac{1}{N_s} \langle \tau^{xx} \rangle$ in [37]), is given by

$$\mathcal{T} = \frac{q_e^2}{N_s} \sum_{k\sigma} \left(\frac{d^2 \varepsilon_{\vec{k}}}{dk_x^2} \right) \langle \tilde{C}_{\vec{k}\sigma}^\dagger \tilde{C}_{\vec{k}\sigma} \rangle, \quad (21)$$

It can be seen that \mathcal{T} is related to the f-sumrule for the optical conductivity

$$\int_{-\infty}^{\infty} \frac{d\omega}{\pi} \text{Re } \sigma(\omega) = \mathcal{T}. \quad (22)$$

When parabolic bands $\varepsilon_{\vec{k}} = k^2/(2m)$ are used, we find at all \vec{q} the simple result

$$\mathcal{T} = \left(\frac{nq_e^2}{m} \right), \quad (23)$$

where $n = N/N_s$ is the electron density [38]. Combining Eq. (17, 18), we find

$$\frac{d^2}{d\tau^2} \chi_{\rho\rho}(\vec{q}, \tau) = -\delta(\tau) N_s \kappa(\vec{q}) + \chi_{WW}(\vec{q}, \tau), \quad (24)$$

Multiplying both sides by $e^{i\Omega_\nu \tau}$ and integrating over τ as in Eq. (B.8) we find

$$\chi_{\rho\rho}(\vec{q}, i\Omega_\nu) = \frac{1}{\Omega_\nu^2} (N_s \kappa(\vec{q}) - \chi_{WW}(\vec{q}, i\Omega_\nu)). \quad (25)$$

The large Ω behaviour is determined by the first term, since χ vanishes there, and leads to the important plasma sum-rule discussed below in Eq. (E.6, E.8, E.9, E.11, E.12).

Analogous relations can be derived for real frequencies using the definitions in Eq. (B.1). We write Eq. (17) and Eq. (18) directly in ω space as

$$(\omega) \chi_{\rho\rho}(\vec{q}, \omega) = i \chi_{W\rho}(\vec{q}, \omega) = -i \chi_{\rho W}(\vec{q}, \omega) \quad (26)$$

$$(\omega) \chi_{W\rho}(\vec{q}, \omega) = i N_s \kappa(\vec{q}) - i \chi_{WW}(\vec{q}, \omega) \quad (27)$$

where κ is defined in Eq. (19). It is clear that these relations in ω can be obtained from Eq. (25) by analytically continuing the Matsubara frequency $i\Omega_\nu \rightarrow \omega + i0^+$. Combining these we get

$$\chi_{\rho\rho}(\vec{q}, \omega) = -\frac{1}{\omega^2} (N_s \kappa(\vec{q}) - \chi_{WW}(\vec{q}, \omega)). \quad (28)$$

which is analytically continued version of Eq. (25) for real frequencies.

We note the relationship between the reducible susceptibility $\chi_{\rho\rho}$ and the dielectric function $\varepsilon(\vec{q}, \omega)$

$$\frac{1}{\varepsilon(\vec{q}, \omega)} = 1 - \frac{V(\vec{q})}{q_e^2} \chi_{\rho\rho}(\vec{q}, \omega). \quad (29)$$

This is easily established [5] from linear response theory. From Eq. (28) we note that we can compute $\varepsilon(\vec{q}, \omega)$ directly from $\chi_{\rho\rho}(\vec{q}, \omega)$, or alternately from $\chi_{WW}(\vec{q}, \omega)$. When done exactly, these alternate formulas must of course coincide, but they offer important possibilities for approximations that we shall pursue below.

4 Irreducible susceptibilities and alternate expressions for $\varepsilon(\vec{q}, \omega)$

We turn to the irreducible susceptibilities $\tilde{\chi}_{\rho\rho}$ and $\tilde{\chi}_{W\rho}$, which are more convenient since they already contain to a large extent the effects of the long ranged part of the Coulomb interaction. In the electron gas problem these susceptibilities can be rigorously defined diagrammatically by using screened vertex functions [5]. We can easily generalize the treatment in Nozières to conventional electrons in a tight binding model. This corresponds to Eq. (2) without the H_J and with conventional electrons replacing the Gutzwiller projected electron operators $\tilde{C}_{j\sigma}$. With Gutzwiller projection the entire calculation is non-trivial since the definition of vertex functions is beset with technical difficulties described elsewhere [18, 19]. In Appendix-(D) we present a workaround, avoiding the use of vertex functions entirely and instead using the relationship between correlation functions directly. The final relationships between the two sets of susceptibilities, valid for a tight binding band of non-canonical electrons at arbitrary \vec{q}, ω , are exactly the same as that for conventional electrons.

We denote the pair of subscripts $\{\rho, W\}$ by a symbol μ (or ν), and introduce the irreducible susceptibilities $\tilde{\chi}_{\mu\nu}(\vec{q}, \omega)$. Rules for calculating the reducible and irreducible susceptibilities from taking functional derivatives of the Green's functions are provided in the Appendix-(C) and Appendix-(D). The relationships between the irreducible and the reducible susceptibilities are compactly given by (see Eq. (D.9))

$$\chi_{\mu\nu}(q) = \tilde{\chi}_{\mu\nu}(q) - \frac{1}{q_e^2} V(\vec{q}) \tilde{\chi}_{\mu\rho}(q) \chi_{\rho\nu}(q). \quad (30)$$

This can be solved for all the components and displays the screened nature of the resulting susceptibilities. The density-density response $\chi_{\rho\rho}$ is simplest since all terms on the right have the same subscripts. Gathering terms $\chi_{\mu\nu}(q)$ on the left, we find

$$\chi_{\rho\rho}(q) = \frac{\tilde{\chi}_{\rho\rho}(q)}{1 + \frac{1}{q_e^2} V(\vec{q}) \tilde{\chi}_{\rho\rho}(\vec{q}, \omega)}. \quad (31)$$

Using Eq. (29), dielectric function is given in terms of the irreducible susceptibility by

$$\varepsilon(q) \equiv \varepsilon(\vec{q}, \omega) = 1 + \frac{1}{q_e^2} V(\vec{q}) \tilde{\chi}_{\rho\rho}(\vec{q}, \omega), \quad (32)$$

with the Coulomb potential given by Eq. (6, 7). Proceeding similarly we find the other three susceptibilities in terms of their screened counterparts. With $q = (\vec{q}, \omega)$ the relationships between the four susceptibilities are given by

$$\chi_{\rho\rho}(q) = \frac{\tilde{\chi}_{\rho\rho}(q)}{\varepsilon(q)} \quad (33)$$

$$\chi_{\rho W}(q) = \frac{\tilde{\chi}_{\rho W}(q)}{\varepsilon(q)}, \quad (34)$$

$$\chi_{W\rho}(q) = \frac{\tilde{\chi}_{W\rho}(q)}{\varepsilon(q)}, \quad (35)$$

$$\chi_{WW}(q) = \tilde{\chi}_{WW}(q) - \frac{V(\vec{q})}{q_e^2 \varepsilon(q)} \tilde{\chi}_{W\rho}(q) \tilde{\chi}_{\rho W}(q). \quad (36)$$

It is worth noting the connection between these results and the equations presented by Nozières [5] for the homogeneous electron gas — denoted by a prefix “N”. The vertex W (see Eq. (9)) replaces the (longitudinal) current vertex $(-i) \frac{\vec{q} \cdot \vec{k}}{m}$ in Ref. [5], who chooses \vec{q} along the z (or 3) axis and denotes $\frac{k_z}{m}$ by “3”. Our pair of operators map as $\{\rho \rightarrow 4, W \rightarrow 3\}$ to those of Nozières. Our susceptibilities $\chi_{\mu,\nu}$ are $\frac{i}{2\pi\Omega} \times S_{\alpha,\beta}$ of Nozières. Our dielectric function in Eq. (32) corresponds to his Eq. (N-6.170), our Eq. (31, 34, 35, 36) correspond to Eq. (N-6.168).

We next study the charge conservation laws for the screened susceptibilities $\tilde{\chi}_{\mu\nu}$, combining the conservation relations Eq. (26, 27) for the unscreened susceptibilities and the relations (Eq. (31, 34, 35, 36)). Now using $\tilde{\chi}_{\rho\rho} = \chi_{\rho\rho} \times \varepsilon$ and Eq. (34) we write

$$(\omega) \tilde{\chi}_{\rho\rho}(\vec{q}, \omega) = i \tilde{\chi}_{W\rho}(\vec{q}, \omega) = -i \tilde{\chi}_{\rho W}(\vec{q}, \omega). \quad (37)$$

For the next step we rearrange Eq. (28) as

$$N_s \kappa(\vec{q}) = \chi_{WW}(\vec{q}, \omega) - (\omega^2) \chi_{\rho\rho}(\vec{q}, \omega),$$

and substitute the screening equations Eq. (30), Eq. (34), and Eq. (35) for the right hand side. This yields

$$\begin{aligned} N_s \kappa(\vec{q}) &= \tilde{\chi}_{WW}(\vec{q}, \omega) - (\omega^2) \tilde{\chi}_{\rho\rho}(\vec{q}, \omega) \\ &+ \frac{V(\vec{q})}{q_e^2} \left((\omega)^2 \chi_{\rho\rho}(\vec{q}, \omega) \tilde{\chi}_{\rho\rho}(\vec{q}, \omega) - \tilde{\chi}_{W\rho}(\vec{q}, \omega) \chi_{\rho W}(\vec{q}, \omega) \right). \end{aligned} \quad (38)$$

We now use the conservation laws Eq. (26) $(\omega) \chi_{\rho\rho} = -i \chi_{\rho W}$, and Eq. (37) $(\omega) \tilde{\chi}_{\rho\rho} = i \tilde{\chi}_{W\rho}$. This shows that the second term in Eq. (38) vanishes identically! We thus find the exact result

$$\tilde{\chi}_{\rho\rho}(\vec{q}, \omega) = \frac{1}{\omega^2} \left(\tilde{\chi}_{WW}(\vec{q}, \omega) - N_s \kappa(\vec{q}) \right), \quad (39)$$

as the screened version of Eq. (28). At large $|\omega| \gg t$, since $\tilde{\chi}_{WW}(\vec{q}, \omega) \rightarrow 0$, we find the important asymptotic behaviour for the real part

$$\lim_{\omega \gg t} \tilde{\chi}_{\rho\rho}(\vec{q}, \omega) = -\frac{N_s \kappa(\vec{q})}{\omega^2}. \quad (40)$$

For any generic \vec{q} we must obtain a finite static limit of $\tilde{\chi}_{\rho\rho}$, which requires an exact cancellation between the two terms in the bracket, i.e.

$$\tilde{\chi}_{WW}(\vec{q}, 0) = N_s \kappa(\vec{q}), \quad (41)$$

and therefore can alternately write

$$\tilde{\chi}_{\rho\rho}(\vec{q}, \omega) = \frac{N_s \kappa(\vec{q})}{\omega^2} \left(\tilde{\chi}_{WW}(\vec{q}, \omega) / \tilde{\chi}_{WW}(\vec{q}, 0) - 1 \right), \quad (42)$$

Combining Eq. (39) we get an expression for $\varepsilon(\vec{q}, \omega)$, alternate to Eq. (32)

$$\varepsilon(\vec{q}, \omega) = 1 + \frac{1}{q_e^2 \omega^2} V(\vec{q}) \left(\tilde{\chi}_{WW}(\vec{q}, \omega) - N_s \kappa(\vec{q}) \right). \quad (43)$$

The expressions Eq. (32, 43) are the twin Nozières formulas referred to in the introduction. The formal derivation shows that if the two expressions are evaluated exactly, then they must coincide. Approximations are not guaranteed to retain their equivalence. In certain classes of approximate calculations they do agree. For example the standard random phase approximation (RPA) uses the non-interacting Green's functions G_0 , and the vertex is the bare one. The two susceptibilities are found from the bubble diagrams [5]

$$\tilde{\chi}_{\rho\rho}^{(0)}(\vec{q}, i\Omega_\nu) = -q_e^2 \sum_{k\sigma} G_0(k) G_0(k+q) = 2q_e^2 \sum_{\vec{k}} \frac{f_{\vec{k}} - f_{\vec{k}+\vec{q}}}{\varepsilon_{\vec{k}+\vec{q}} - \varepsilon_{\vec{k}} - i\Omega_\nu}, \quad (44)$$

$$\begin{aligned} \tilde{\chi}_{WW}^{(0)}(\vec{q}, i\Omega_\nu) &= -q_e^2 \sum_{k\sigma} G_0(k) G_0(k+q) (\varepsilon_{\vec{k}} - \varepsilon_{\vec{k}+\vec{q}})^2 \\ &= 2q_e^2 \sum_{\vec{k}} \frac{f_{\vec{k}} - f_{\vec{k}+\vec{q}}}{\varepsilon_{\vec{k}+\vec{q}} - \varepsilon_{\vec{k}} - i\Omega_\nu} (\varepsilon_{\vec{k}} - \varepsilon_{\vec{k}+\vec{q}})^2 \end{aligned} \quad (45)$$

In this case the validity of Eq. (42) can be shown by multiplying Eq. (44) by $(i\Omega_\nu)^2$, followed by the use of partial fractions. This process reduces it to Eq. (45) plus a term equivalent to $N_s q_e^2 \tau(q)$.

In the case of canonical electrons, we can define vertex functions suitably, and make approximations for the vertex as well as the Green's functions in a consistent way [5, 9] so that the Ward-Takahashi identities are satisfied. Such approximations guarantee the equivalence of the approximate versions of Eq. (32, 43). The RPA described above is an example of such an approximation, this scheme trivially satisfies the Ward-Takahashi identities.

5 Calculating the Approximate Dielectric Function

The main problem of interest in this work is the t - J - V_C model. Here the short ranged Coulomb interactions lead to a Mott-Hubbard type insulating state at half filling, and doping such a state with holes leads to a metallic state of a very unusual — endowed with a small quasiparticle weight. Adding long ranged Coulomb interactions to this state poses a considerable difficulty. While we are able to obtain a fairly sophisticated single electron Green's function \mathcal{G} from the ECFL theory [18], the two particle response functions are currently unreliable. This is a difficult task even for the simpler case of canonical electrons, and has led to a variety of beyond-RPA type approximations [36]. For Gutzwiller projected electrons, it is indeed a formidable task. In this situation, the availability of the two alternate formulas Eq. (32, 43) is very helpful. We can compute the susceptibilities $\tilde{\chi}_{\rho\rho}(\vec{q}, \omega)$ and $\tilde{\chi}_{WW}(\vec{q}, \omega)$ at all $\{\vec{q}, \omega\}$, using only the above \mathcal{G} within a bubble scheme \mathcal{GG} as described below in Eq. (61, 62). Being approximate, these two estimates differ in general, but provide complementary perspective on the dielectric response at various \vec{q}, ω . By comparing these estimates with known (exact) limiting behaviour of the susceptibility detailed in Appendix-(E), we can ascertain their respective regimes of validity. This provides us with the possibility of combining the two formulas, to obtain an approximate answer whose broad characteristics are known beforehand.

5.1 Formula for irreducible susceptibility in terms of its self-energy $\Psi(\vec{q}, \omega)$

We begin with a novel representation for the susceptibility using the freedom to define suitable generalized self-energies of Green's functions, as discussed in [27–29]. We start from the high frequency moment expansion Eq. (F.8), in inverse powers of ω^2 as discussed in Appendix-(F.2). This series can be formally rewritten in a continued fraction representation following Mori [28, 29] as

$$\frac{1}{q_e^2 N_s} \tilde{\chi}_{\rho\rho}(\vec{q}, \omega) = \frac{\beta_1(\vec{q})}{\omega^2 - \alpha_1(\vec{q}) - \Sigma_\chi^{(0)}(\vec{q}, \omega)} \quad (46)$$

$$\Sigma_\chi^{(0)}(\vec{q}, \omega) = \frac{\beta_2(\vec{q})}{\omega^2 - \alpha_2(\vec{q}) - \Sigma_\chi^{(1)}(\vec{q}, \omega)} \quad (47)$$

⋮

where $\beta_1 = -\tilde{\omega}_q^{(1)}$ is the negative of the first moment of frequency Eq. (F.10, F.14), and $\Sigma_\chi^{(m)}(\vec{q}, \omega)$ with $m = 0, 1, \dots$ represent the successive “self-energies”. They are characterized by the property that for $\omega \gg t$ they behave as $\Sigma_\chi^{(m)}(\vec{q}, \omega) \sim \frac{\beta_{m+2}}{\omega^2}$, and thus vanish. The coefficients α_m, β_m are functions of \vec{q} and can be found in principle, in terms of the frequency moments. It is more convenient for our purpose to rewrite Eq. (46) in by eliminating α_1 in favor of the static limit of $\Sigma_\chi^{(0)}$, and using $\beta_1 = -\tilde{\omega}_q^{(1)}$. This leads to

$$\frac{1}{q_e^2 N_s} \tilde{\chi}_{\rho\rho}(\vec{q}, \omega) = \left(\frac{q_e^2 N_s}{\tilde{\chi}_{\rho\rho}(\vec{q}, 0)} - \frac{\omega^2}{\tilde{\omega}^{(1)}(\vec{q})} + \frac{1}{\tilde{\omega}^{(1)}(\vec{q})} \left(\Sigma_\chi^{(0)}(\vec{q}, \omega) - \Sigma_\chi^{(0)}(\vec{q}, 0) \right) \right)^{-1}. \quad (48)$$

We can simplify the notation by defining a new self-energy type function

$$\Psi(\vec{q}, \omega) = \frac{1}{\tilde{\omega}^{(1)}(\vec{q})} \left(\Sigma_\chi^{(0)}(\vec{q}, 0) - \Sigma_\chi^{(0)}(\vec{q}, \omega) \right), \quad (49)$$

with $\tilde{\omega}^{(1)}(\vec{q})$ detailed in Eq. (F.10, F.12). The irreducible susceptibility is now given by

$$\frac{1}{q_e^2 N_s} \tilde{\chi}_{\rho\rho}(\vec{q}, \omega) = \left(\frac{q_e^2 N_s}{\tilde{\chi}_{\rho\rho}(\vec{q}, 0)} - \frac{\omega^2}{\tilde{\omega}^{(1)}(\vec{q})} - \Psi(\vec{q}, \omega) \right)^{-1}. \quad (50)$$

This self-energy Ψ can be found from $\tilde{\chi}_{\rho\rho}(\vec{q}, \omega)$, if the latter is known, by inversion of Eq. (50), and can be expressed formally in terms of the higher moments $\tilde{\omega}^{(2j+1)}(\vec{q})$ using Eq. (F.8) [27–29]. The self energy vanishes in the static limit by construction

$$\Psi(\vec{q}, \omega)|_{\omega \rightarrow 0} = 0, \quad (51)$$

and has a finite high frequency limit (from the first term in Eq. (49)).

We note that from the Lehmann representation of $\tilde{\chi}_{\rho\rho}(\vec{q}, \omega)$ that the $\Sigma^{(m)}$ in complex ω are analytic everywhere except the real axis. This implies that all singularities are located on the real axis, and hence these can be further represented in the form

$$\Sigma_{\chi}^{(0)}(\vec{q}, \omega) = -\frac{1}{\pi} \int_{-\infty}^{\infty} d\nu \frac{\text{Im} \Sigma_{\chi}^{(0)}(\vec{q}, \nu)}{\omega - \nu + i\eta} \quad (52)$$

where $\eta = 0^+$. Using the fact that $\Sigma_{\chi}^{(0)}(\vec{q}, 0)$ and $\tilde{\chi}_{\rho\rho}(\vec{q}, 0)$ are real, it follows from Eq. (50) that

$$\text{Im} \Psi(\vec{q}, \omega) = -q_e^2 N_s \text{Im} \tilde{\chi}_{\rho\rho}^{-1}(\vec{q}, \omega). \quad (53)$$

Using the analyticity of Ψ in the upper half complex ω plane, together with Eq. (51), we obtain an expression for Ψ in terms of the imaginary part of the inverse susceptibility

$$\Psi(\vec{q}, \omega) = (q_e^2 N_s) \left(\frac{1}{\pi} \int_{-\infty}^{\infty} d\nu \frac{\text{Im} \tilde{\chi}_{\rho\rho}^{-1}(\vec{q}, \nu)}{\omega - \nu + i\eta} + \frac{1}{\pi} \int_{-\infty}^{\infty} d\nu \frac{\text{Im} \tilde{\chi}_{\rho\rho}^{-1}(\vec{q}, \nu)}{\nu} \right). \quad (54)$$

Here the second term is expected to be finite due to the odd-ness in frequency of $\text{Im} \tilde{\chi}_{\rho\rho}^{-1}(\vec{q}, \nu)$. It follows from Eq. (53) that $\text{Im} \Psi(\vec{q}, \omega)$ is odd in ω while Eq. (54) says that $\text{Re} \Psi(\vec{q}, \omega)$ is even in ω .

In summary the susceptibility $\tilde{\chi}_{\rho\rho}(\vec{q}, \nu)$ is determined in Eq. (50) by the self energy $\Psi(\vec{q}, \omega)$ satisfying Eq. (51) and Eq. (54), together with two functions of \vec{q} only: (a) the static susceptibility $\tilde{\chi}_{\rho\rho}(\vec{q}, 0)$ and (b) the moment $\tilde{\omega}^{(1)}(\vec{q})$ (with dimensions of frequency). The latter is calculable for all \vec{q} in terms of equal time correlations from Eq. (F.12).

Separating $\Psi = \Psi' + i\Psi''$, we can write the complex susceptibility Eq. (50) conveniently as

$$\frac{1}{q_e^2 N_s} \tilde{\chi}_{\rho\rho}(\vec{q}, \omega) = \left(\frac{1}{\tilde{\omega}^{(1)}(\vec{q})} \{ \Omega^2(\vec{q}, \omega) - \omega^2 \} - i\Psi''(\vec{q}, \omega) \right)^{-1}, \quad (55)$$

and hence

$$\frac{1}{q_e^2 N_s} \text{Im} \tilde{\chi}_{\rho\rho}(\vec{q}, \omega) = \frac{[\tilde{\omega}^{(1)}(\vec{q})]^2 \Psi''(\vec{q}, \omega)}{[\tilde{\omega}^{(1)}(\vec{q}) \Psi''(\vec{q}, \omega)]^2 + \{ \Omega^2(\vec{q}, \omega) - \omega^2 \}^2}. \quad (56)$$

In these expressions the characteristic energy scale Ω is given by

$$\Omega^2(\vec{q}, \omega) = \tilde{\omega}^{(1)}(\vec{q}) \left(\frac{d\mu}{dn} \gamma(\vec{q}) - \Psi'(\vec{q}, \omega) \right) \quad (57)$$

$$\gamma(\vec{q}) = \frac{\tilde{\chi}_{\rho\rho}(0, 0)}{\tilde{\chi}_{\rho\rho}(\vec{q}, 0)}, \quad \gamma(0) = 1, \quad (58)$$

and we made use of the exact result Eq. (E.1) to express the static limit of the susceptibility in terms of the thermodynamic variable $\frac{d\mu}{dn}$. Recall that the compressibility $\chi_{comp} = \frac{1}{2n(0)} \frac{dn}{d\mu} \chi_{comp}^{(non)}$, where $n(0)$ is the density of states per site per spin, and hence this representation also satisfies the compressibility sum-rule Eq. (E.1).

From Eq. (56) we see that the peaks in $\text{Im} \tilde{\chi}_{\rho\rho}(\vec{q}, \omega)$ are located at the roots of $\omega^2 = \Omega^2(\vec{q}, \omega)$. As $\vec{q} \rightarrow 0$ the relevant frequency is low and hence the root is approximately located at the energy scale $\Omega(\vec{q}, 0)$. We denote this scale as

$$\Omega_p(\vec{q}) = \Omega(\vec{q}, 0) = \sqrt{\tilde{\omega}^{(1)}(\vec{q}) \frac{d\mu}{dn} \gamma(\vec{q})}. \quad (59)$$

We also note that the width of the peak is given by

$$\Gamma_p(\vec{q}) = \sqrt{\tilde{\omega}^{(1)}(\vec{q}) \Psi''(\vec{q}, \Omega_p(\vec{q}))}. \quad (60)$$

In Fig. (8), we present typical results for $\tilde{\omega}^{(1)}(\vec{q}) \Psi''(\vec{q}, \omega)$. An explicit expression for the important energy scale $\Omega_p(\vec{q})$ is given later in Section-(5.5) and Eq. (77). In those sections we also provide an alternate and direct argument that obtains this scale, starting from the normalized spectral function of density fluctuations $\varphi(\vec{q}, \omega)$ Eq. (78). Experimentally $\Omega_p(\vec{q})$ can be inferred from a turn-around feature observed in the plots of $\text{Im} \tilde{\chi}_{\rho\rho}(\vec{q}, \omega)$, as in Fig. (10, 11), and is displayed in Fig. (12).

The representation Eq. (50) also exactly satisfies the known high ω behavior Eq. (F.8), and therefore reproduces the correct plasma frequency Eq. (E.7). It should also be clear that with obvious changes to the variables, the above formulas Eq. (50, 55) can be useful for other physical situations such as the homogeneous electron gas etc.

5.2 Calculation of the irreducible susceptibility $\tilde{\chi}_{\rho\rho}(\vec{q}, \nu)$

It is very convenient to calculate the susceptibility starting from formulas Eq. (50). The input variables in Eq. (50, 55) are found from the ECFL theory, using suitable approximations described next. We make extensive use of the *bubble approximation*, where in taking the derivative with respect to the external potential in Eq. (D.7), the \mathcal{G} is assumed to depend on this potential *only* through the explicit terms as in Eq. (D.5), and the implicit dependence via the other factors are thrown out. For $\tilde{\chi}_{\rho\rho}$ we find an approximate expression from this bubble approximation

$$\tilde{\chi}_{\rho\rho}^{\text{Bub}}(\vec{q}, \omega) = -q_e^2 \sum_{k\sigma} \mathcal{G}(k) \mathcal{G}(k+q), \quad (61)$$

and evaluating $\tilde{\chi}_{WW}$ within the bubble approximation

$$\tilde{\chi}_{WW}^{\text{Bub}}(\vec{q}, \omega) = -q_e^2 \sum_{k\sigma} \mathcal{G}(k) \mathcal{G}(k+q) (\varepsilon_k - \varepsilon_{k+q})^2. \quad (62)$$

Using the spectral representation Eq. (A.11) for \mathcal{G} the latter reduces to

$$\begin{aligned} \tilde{\chi}_{WW}^{\text{Bub}}(\vec{q}, \omega) &= 2q_e^2 \sum_k (\varepsilon_k - \varepsilon_{k+q})^2 \\ &\times \int_{\nu_1 \nu_2} \frac{f(\nu_1) - f(\nu_2)}{\nu_2 - \nu_1 - \omega - i0^+} A(k, \nu_1) A(k+q, \nu_2), \end{aligned} \quad (63)$$

where $\int_{\nu} = \int_{-\infty}^{\infty} d\nu$. The density response $\tilde{\chi}_{\rho\rho}^{\text{Bub}}(\vec{q}, \omega)$ is found by dropping the factor $(\varepsilon_k - \varepsilon_{k+q})^2$ in this formula. The spectral functions in our model (see Fig. (1)) consist of a quasiparticle part with a much reduced weight $Z \ll 1$, and an extended background part. The indicated integrations can be performed numerically.

Our two starting points are susceptibilities found from these bubble estimates and Eq. (42)

$$\tilde{\chi}_A(\vec{q}, \omega) = \tilde{\chi}_{\rho\rho}^{\text{Bub}}(\vec{q}, \omega) \quad (64)$$

$$\tilde{\chi}_B(\vec{q}, \omega) = \frac{N_s \kappa(\vec{q})}{\omega^2} \left(\tilde{\chi}_{WW}^{\text{Bub}}(\vec{q}, \omega) / \tilde{\chi}_{WW}^{\text{Bub}}(\vec{q}, 0) - 1 \right). \quad (65)$$

For $\tilde{\chi}_B$ we verify that $\tilde{\chi}_{WW}^{\text{Bub}}(\vec{q}, 0)$ agrees closely with $N_s \kappa(\vec{q})$, calculated independently using a single Green's function \mathcal{G} from Eq. (19), at all \vec{q} (see Fig. (6)). The estimate $\tilde{\chi}_A$ provides a reasonable estimate in the static limit for the susceptibility. The magnitude of the compressibility, found by taking the $\vec{q} \rightarrow 0$ limit, is much smaller than the band value, as seen in Fig. (3). It is comparable for most densities to that found from thermodynamical evaluation of $\frac{dn}{d\mu}$ (see Fig. (3)). At finite \vec{q} its shape resembles that of the band susceptibility (see Fig. (4)). The imaginary part of $\tilde{\chi}_A$ shows a quasiparticle contribution of the type $\chi'' \propto \frac{\pi\omega}{|\vec{q}|v_F}$ for very small $\omega < |\vec{q}|v_F Z$. For larger ω , it has a broad contribution from the background spectral functions, but does not give the first moment of frequency, and is therefore not satisfactory.

The estimate $\tilde{\chi}_B$ is expected to be satisfactory at finite (high) frequencies since it is constructed to satisfy the first moment of frequency in the high ω limit. However at low ω it does not capture the quasiparticle contribution discussed above. Further the static limit — found from the $\mathcal{O}(\omega^2)$ limiting behavior of $\tilde{\chi}_{WW}^{\text{Bub}}(\vec{q}, \omega)$ — does not display the behavior expected for an incompressible system discussed above. Thus the two estimates are successful in almost non-overlapping regimes of frequency.

Before proceeding we note that the two expressions Eq. (64, 65) lead to two different self energies

$$\Psi_A(\vec{q}, \omega) + \frac{\omega^2}{\tilde{\omega}_A^{(1)}(\vec{q})} = \frac{N_s q_e^2}{\tilde{\chi}_A(\vec{q}, 0)} - \frac{N_s q_e^2}{\tilde{\chi}_A(\vec{q}, \omega)} \quad (66)$$

$$\Psi_B(\vec{q}, \omega) + \frac{\omega^2}{\tilde{\omega}_B^{(1)}(\vec{q})} = \frac{N_s q_e^2}{\tilde{\chi}_B(\vec{q}, 0)} - \frac{N_s q_e^2}{\tilde{\chi}_B(\vec{q}, \omega)}. \quad (67)$$

The first frequency moment $\tilde{\omega}_B^{(1)}(\vec{q})$ in the second equation Eq. (67) is in fact exact, i.e. $\tilde{\omega}_B^{(1)}(\vec{q}) = \tilde{\omega}^{(1)}(\vec{q})$, as explained above. The corresponding frequency $\tilde{\omega}_A^{(1)}(\vec{q})$ is not correct, and we show that it is possible to avoid using it altogether.

Consider the approximate susceptibility $\tilde{\chi}^{(I)}$ combining the two susceptibilities $\tilde{\chi}_A, \tilde{\chi}_B$ as

$$\tilde{\chi}^{(I)}(\vec{q}, \omega) = \left\{ \frac{1}{\tilde{\chi}_A(\vec{q}, 0)} - \frac{1}{\tilde{\chi}_B(\vec{q}, 0)} + \frac{1}{\tilde{\chi}_B(\vec{q}, \omega)} \right\}^{-1} \quad (68)$$

$$= N_s q_e^2 \left\{ \frac{N_s q_e^2}{\tilde{\chi}_A(\vec{q}, 0)} - \frac{\omega^2}{\tilde{\omega}^{(1)}(\vec{q})} - \Psi_B(\vec{q}, \omega) \right\}^{-1}. \quad (69)$$

It is readily seen from the arguments given above, to give the correct plasma frequency as well as the correct static limit, while respecting the strong local correlations. It therefore serves as a reasonable approximation over the entire frequency domain.

A feature that is missing from $\tilde{\chi}^{(I)}$ in Eq. (69), is the quasi-particle contribution. This was present in Eq. (64), but was left out in Eq. (69) since we threw out all the frequency dependence of $\tilde{\chi}_A$. We can incorporate this contribution, again approximately, by making a correction to Ψ_B taken from Ψ_A . Inspection shows that for small \vec{q}, ω the quasiparticle feature in $\tilde{\chi}_A$ arises from a contribution $\text{Im } \Psi_A \propto \frac{\omega}{|\vec{q}|v_f}$. It is analogous to the familiar correction that arises in the Lindhard function from quasiparticles [5–7]. This quasiparticle contribution leads to $|\text{Im } \Psi_A(\vec{q}, \omega)| > |\text{Im } \Psi_B(\vec{q}, \omega)|$ for small enough ω at a fixed \vec{q} , while for larger $|\omega|$ we find $|\text{Im } \Psi_B(\vec{q}, \omega)| \gg |\text{Im } \Psi_A(\vec{q}, \omega)|$. To further refine the approximation, we keep this observation in mind and add the incremental $\delta\Psi_{QP}(\vec{q}, \omega)$ containing the quasiparticle damping to Ψ_B ,

$$\tilde{\chi}^{(II)}(\vec{q}, \omega) = N_s q_e^2 \left\{ \frac{N_s q_e^2}{\tilde{\chi}_A(\vec{q}, 0)} - \frac{\omega^2}{\tilde{\omega}^{(1)}(\vec{q})} - \Psi_B(\vec{q}, \omega) - \delta\Psi_{QP}(\vec{q}, \omega) \right\}^{-1}. \quad (70)$$

Since $\text{Im } \delta\Psi_{QP}$ should add the damping due to quasiparticles, with $\omega > 0$ we choose

$$\text{Im } \delta\Psi_{QP}(\vec{q}, \omega) = \text{Max}\{\text{Im } \Psi_A(\vec{q}, \omega), \text{Im } \Psi_B(\vec{q}, \omega)\} - \text{Im } \Psi_B(\vec{q}, \omega), \quad (71)$$

It is easily seen that $\text{Im } \delta\Psi_{QP}(\vec{q}, \omega)$ vanishes outside the region $|\text{Im } \Psi_A(\vec{q}, \omega)| > |\text{Im } \Psi_B(\vec{q}, \omega)|$. For $\omega < 0$ a similar argument can be used keeping in mind the odd-ness of $\text{Im } \Psi$'s in ω , we use Min instead of Max in Eq. (71). The real part of $\delta\Psi_{QP}$ can be calculated using the Kramers-Kronig relation, i.e. by taking the real part in Eq. (54)

$$\text{Re } \delta\Psi_{QP}(\vec{q}, \omega) = -\mathcal{P} \frac{1}{\pi} \int_{-\infty}^{\infty} d\nu \frac{\text{Im } \delta\Psi_{QP}(\vec{q}, \nu)}{\omega - \nu} - \frac{1}{\pi} \int_{-\infty}^{\infty} d\nu \frac{\text{Im } \delta\Psi_{QP}(\vec{q}, \nu)}{\nu}, \quad (72)$$

whereby we guarantee that $\delta\Psi_{QP}(\vec{q}, 0) = 0$.

On further separating the complex self-energies, these two approximate susceptibilities Eq. (69, 70) lead to expressions analogous to Eq. (55), with the same static susceptibility Eq. (58) but slightly different characteristic frequencies Ω in Eq. (57).

With these approximations $\tilde{\chi}^{(I)}(\vec{q}, \omega), \tilde{\chi}^{(II)}(\vec{q}, \omega)$, the 2-d dielectric function can be written in the form

$$\begin{aligned} \varepsilon^{(I,II)}(\vec{q}, \omega) &= 1 + \frac{2\pi q_e^2}{|\vec{q}|a_0^2 N_s q_e^2 \varepsilon_\infty} \tilde{\chi}^{(I,II)}(\vec{q}, \omega) \\ &= 1 + \frac{g_c}{|\vec{q}|a_0} \left(\frac{t}{q_e^2 N_s} \tilde{\chi}^{(I,II)}(\vec{q}, \omega) \right), \end{aligned} \quad (73)$$

where the dimensionless Coulomb constant is defined by

$$g_c = \frac{2\pi q_e^2}{\varepsilon_\infty a_0 t}. \quad (74)$$

With the 2-d lattice constant $a_0 = 3.81\text{\AA}$, $t = 0.45\text{eV}$ and $\varepsilon_\infty = 1.76$, we get $g_c \sim 30.0$. Since these basic parameters can vary somewhat, we present results for $g_c = 10, 50, 100$ in the following.

5.3 Calculations and Results

We calculate the Green's functions using the set of formulas summarized in Appendix-(A) Eq. (A.3–A.9), employing the set of band and model parameters

$$t = 0.45\text{eV}, t' = -0.2\text{eV}, J = 0.17\text{eV}, . \quad (75)$$

The system sizes used in most of the presented calculations are

$$N_\omega = 2^{14}, L_x \times L_y = 64 \times 64 \text{ (correlated model)} \quad (76)$$

where N_ω is the number of ω points in the frequency grid and L_x, L_y are the dimensions of the 2-d lattice. For Fig. (17), Fig. (19), as well as the reference uncorrelated model we use bigger spatial grids $L_x \times L_y = 128 \times 128$. We present results at a few representative temperatures, and focus on two densities $n = 0.80$ and $n = 0.85$. These correspond to the over-doped regime and optimally doped cases. As mentioned above, the resistivity tensor, the optical conductivity and spectral functions have been recently published by us in [20, 21], at these and more enlarged set of parameters. Here we concentrate our attention on the density response function $\tilde{\chi}^{(I)}(\vec{q}, \omega)$ and $\tilde{\chi}^{(II)}(\vec{q}, \omega)$ defined in Eq. (64, 65) and the corresponding dielectric functions Eq. (73). We also focus on the corresponding current response functions $\tilde{\chi}_{JJ}(\vec{q}, \omega)$ defined in Eq. (E.14), and the optical conductivity Eq. (E.15, E.17). These variables are relevant for understanding the experiments in [13–15].

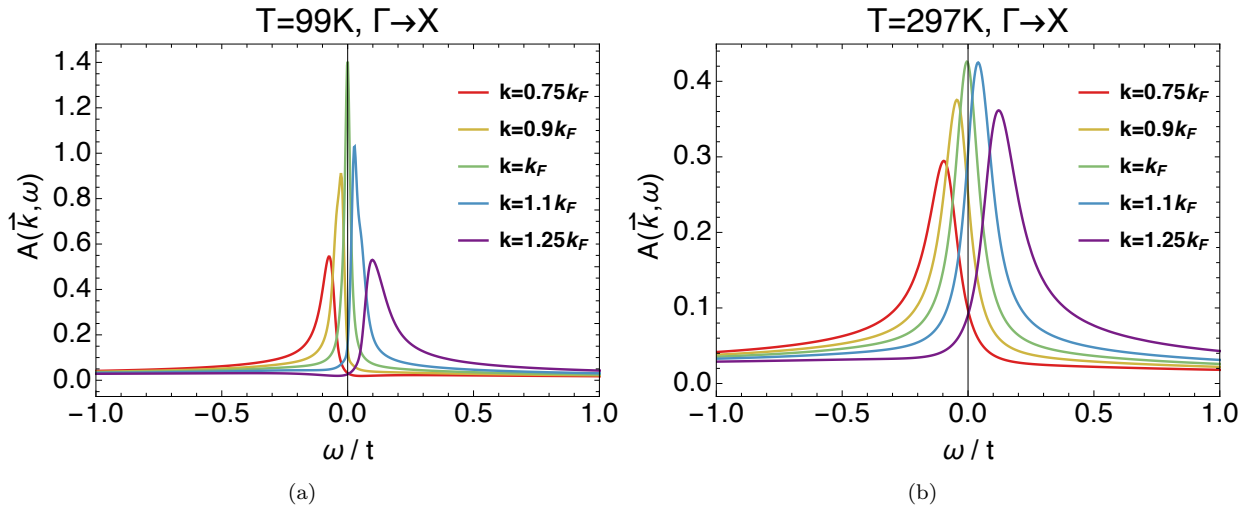


Figure 1: The (single) electronic spectral functions for the ECFL Green's function at two temperatures: (a) $T = 99\text{K}$ and (b) $T = 297\text{K}$ at $n = 0.85$. The Fermi wave vector is $k_F a_0 = 1.36$, and the quasiparticle weight is $Z = 0.06, 0.09$ for $T = 99\text{K}$ and $T = 297\text{K}$ respectively. The spectral width depends sensitively on T . This thermal sensitivity is a characteristic of the ECFL theory, where the effective Fermi temperature is much suppressed from the band value. The reduced quasiparticle weight is also reflected in Fig. (2).

5.4 Basic results

We now present the results from this formalism. We begin with the electronic spectral function $A(\vec{k}, \omega)$ obtained by solving for the ECFL Green's function in Fig. (1). The figure is at the density $n = 0.85$ and at two temperatures $T = 99\text{K}$ and $T = 297\text{K}$. The quasiparticle weight is seen to be very small $Z = 0.06, 0.09$ for $T = 99\text{K}$ and $T = 297\text{K}$ respectively. The area sum-rule for the lower Hubbard band spectral function reads as: $\int d\omega A(\vec{k}, \omega) = 1 - \frac{n}{2}$, it is satisfied by depleting the quasiparticle peak, and smearing it over a wide background. This redistribution of weight accounts for the broad and featureless background seen in the spectral functions, it is a reflection of the strong local correlations.

In Fig. (2) we display the momentum distribution function m_k , i.e. $\langle \tilde{C}_{k\uparrow}^\dagger \tilde{C}_{k\uparrow} \rangle$ for correlated electrons, and the analogous band value n_k for uncorrelated electrons at two densities $n = 0.85$ and $n = 0.80$. In the limit of $T \rightarrow 0$ this curve develops a jump of magnitude Z in the distribution at k_F , following the

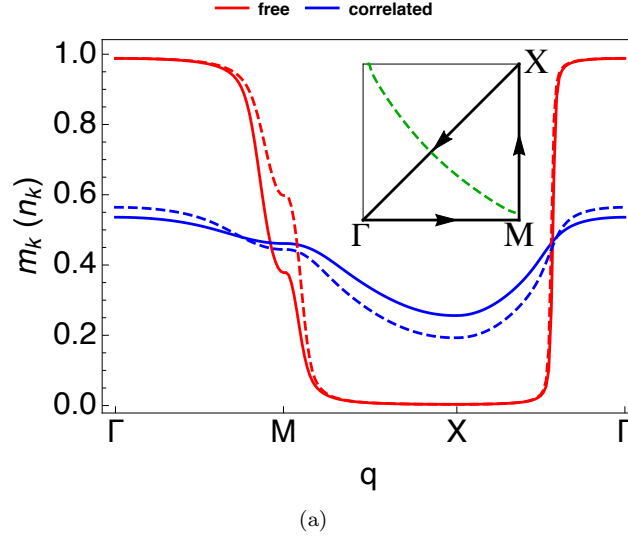


Figure 2: The momentum distribution function m_k for correlated electrons defined as $m_k = \langle \tilde{C}_{k\uparrow}^\dagger \tilde{C}_{k\uparrow} \rangle$ in blue, and the analogous function n_k for uncorrelated electrons ($n_k = \langle c_{k\uparrow}^\dagger c_{k\uparrow} \rangle$) in red, plotted over the Brillouin zone. The solid lines are at $n = 0.85$, and the dashed lines are at $n = 0.80$. Here we used $t = 0.45$, $t' = -0.2$, $J = 0.17$ in units of eV, and $T = 297\text{K}$. And the system size used in the computation is given in Eq. (76). The wave vector q traverses the octant of the Brillouin Zone, with corners $\Gamma = (0, 0)$, $M = (\pi, 0)$, and $X = (\pi, \pi)$ and the green dashed line traces the Fermi surface. A sharp reduction of the quasiparticle weight Z is evident from the flattening of the correlated distribution m_k in this figure.

| n | | Uncorrelated | Correlated |
|------|---|--------------|------------|
| 0.80 | $\langle \cos k_x \rangle_{ave}$ | 0.188847 | 0.056881 |
| | $\langle \cos k_x \cos k_y \rangle_{ave}$ | 0.032757 | 0.00661296 |
| 0.85 | $\langle \cos k_x \rangle_{ave}$ | 0.190954 | 0.0400778 |
| | $\langle \cos k_x \cos k_y \rangle_{ave}$ | 0.018181 | -0.0079378 |

Table 1: The averages used in Eq. (F.14) to calculate $\kappa(\vec{q})$ in Fig. (5). The flattened distribution function m_k in Fig. (2) leads the much smaller values of these angular averages for the correlated metal.

theorem of Migdal. A sharp reduction of the quasiparticle weight Z , noted in Fig. (1), is also evident from the flattening of the correlated distribution m_k .

In Fig. (3) we plot the compressibility using Eq. (E.5) as a function of doping $\delta = 1 - n$. We note that the discrepancy between the static uniform limit of $\tilde{\chi}_{\rho\rho}$ and the thermodynamic result in the sumrule Eq. (E.1) is quite small.

In Fig. (4) we display the momentum dependence of the static susceptibility along the three principal directions at $T = 297\text{K}$ at a density $n = 0.85$. For comparison we also display the bare (uncorrelated) static susceptibility using Eq. (44). Correlations are seen to suppress the magnitudes of the susceptibilities as expected. Somewhat unexpectedly, the relative locations of the three curves, corresponding to different direction in the k -space is strong.

In Fig. (5.a) we display $\kappa(\vec{q})$ Eq. (19) at two densities $n = 0.85$ and $n = 0.8$ using the angular averages shown in Table (1) in Eq. (F.14), and Eq. (F.10, F.12) relating it to the first frequency moment of the structure function $S(\vec{q}, \omega)$. Fig. (5.b) displays the 2-d plasmon spectrum. It is found from κ and Eq. (E.12, E.7, 7). We display the plasma energy along the principal directions in the Brillouin zone. It displays the expected acoustic $\sqrt{|\vec{q}|}$ behavior at low \vec{q} .

In Fig. (6), we compare the computed $\kappa(\vec{q})$, with the static $\tilde{\chi}_{WW}(\vec{q}, 0)/N_s$ obtained from Eq. (62), using the ECFL Green's function. We observe that they are almost identical over the entire Brillouin zone. Their identity is required in order to get a finite limiting behavior for $\tilde{\chi}_{\rho\rho}$ at $\omega = 0$ in Eq. (28). To enforce this behavior exactly in our numerics, we insert the ratio $\kappa(\vec{q})/\tilde{\chi}_{WW}(\vec{q}, 0) \approx 1$ in the second term of Eq. (42).

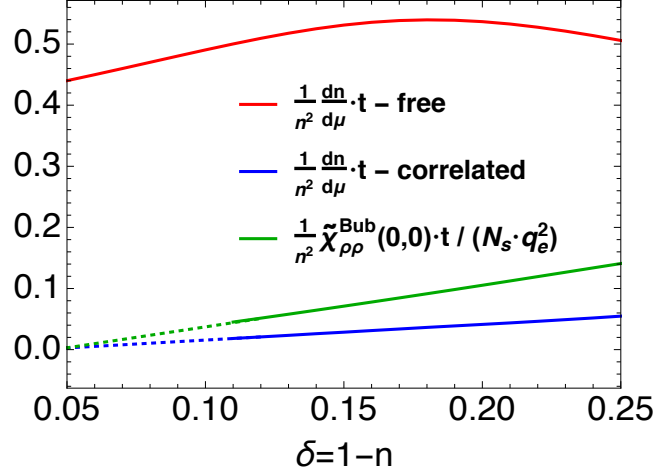


Figure 3: The compressibility Eq. (E.5) versus doping $\delta = 1 - n$, where blue is the correlated case and red is the uncorrelated case. In the correlated case $\frac{dn}{d\mu}$ is found numerically from the computed $\mu(n)$. The dashed lines represent the extrapolation to $\delta = 0$. Correlations are seen to suppress the compressibility as $\delta \rightarrow 0$. The green curve gives the static uniform limit of the susceptibility $\frac{1}{q_e^2 N_s} \lim_{\vec{q} \rightarrow 0} \tilde{\chi}_{\rho\rho}^{\text{Bub}}(\vec{q}, 0)$ (Eq. (61)). If an exact calculation, going beyond the bubble approximation were possible, the corresponding green and blue curves would coincide.

In Fig. (7) panels (a-e) we compare the real and imaginary parts of the self-energies Ψ_A, Ψ_B calculated from Eq. (66, 67). We note that $\text{Im } \Psi_A$ contains a very small quasiparticle contribution as seen in panel (a), characterized by a linear behavior $\Psi'' \propto \frac{\pi\omega}{|\vec{q}|v_F Z}$ for $\omega < |\vec{q}|v_F Z$, while this linear behavior is absent in $\text{Im } \Psi_B$. The construction of $\tilde{\chi}^{(II)}$ in Eq. (70) adds a piece $\delta\Psi_{QP}$ representing the small quasiparticle contribution to the imaginary part of Ψ_B , and recomputes the real part using causality. We display the ω dependence of Ψ_B and $\Psi_B + \delta\Psi_{QP}$ in panels (b), (c), (d) and (f) of Fig. (7).

In Fig. (8) panel (a) we display $\text{Im } \Psi_B$ at different \vec{q} as functions of ω , and note that these collapse to a single curve over the Brillouin zone, when multiplied by $\tilde{\omega}^{(1)}(\vec{q})$. The $\text{Im}\{\Psi_B + \delta\Psi_{QP}\}$ at different \vec{q} differ in the low ω region, due to the presence of the quasi-particle contributions, but do collapse to a single curve at higher frequencies, as seen in panel (b).

In Fig. (9) we compare two approximations for the imaginary part of the irreducible (screened) susceptibilities $\text{Im } \tilde{\chi}^{(I)}$ (solid red line) and $\text{Im } \tilde{\chi}^{(II)}$ (blue dashed lines), i.e., Eq. (69, 70). As expected the quasiparticle contribution at low frequencies is roughly linear in ω .

5.5 Characteristic frequency scale $\Omega_p(\vec{q})$ revisited

We show the density and temperature evolutions of the screened susceptibility approximations $\tilde{\chi}^{(I)}$ (dashed) and $\tilde{\chi}^{(II)}$ (solid) over the ranges $n = 0.8, 0.825, 0.85$ and $T = 99, 198, 295\text{K}$ in the two principle direction $\Gamma \rightarrow X$ [see Fig. (10)] and $\Gamma \rightarrow M$ [see Fig. (11)]. In all cases we observe that the high ω fall off of $\text{Im } \tilde{\chi}$ is $\sim \frac{1}{\omega^2}$, while the curves turn-around at low frequencies to vanish as $\omega \rightarrow 0$. This turn-around occurs at the peak frequency $\Omega_p(\vec{q})$ discussed in Eq. (59), and displayed in Fig. (12). The magnitude of the turn-around frequency $\Omega_p(\vec{q})$, typically a small fraction of t can, depending upon the choice of the hopping parameter t , be very small. We can estimate this further as follows. Using Eq. (57, 59) together with the expression for the first moment $\tilde{\omega}^{(1)}(\vec{q})$ in Eq. (F.12, F.14, F.15) we express $\Omega_p(\vec{q})$ explicitly as a function of \vec{q} . At small \vec{q} this simplifies further to

$$\lim_{\vec{q} \rightarrow 0} \Omega_p(\vec{q}) = |\vec{q}| \sqrt{\frac{\mathcal{T}}{q_e^2} \frac{d\mu}{dn}}, \quad (77)$$

where the velocity $\sqrt{\frac{\mathcal{T}}{q_e^2} \frac{d\mu}{dn}}$ is determined by the ratio of \mathcal{T} Eq. (F.16) that shrinks as the density $n \rightarrow 1$, and the compressibility Fig. (3). We comment further on this turn-around when discussing Fig. (17, 19).

Given the interesting role played by this energy scale $\Omega_p(\vec{q})$, a natural question is whether it has a more direct origin and interpretation. For this purpose we construct a positive definite spectral-shape

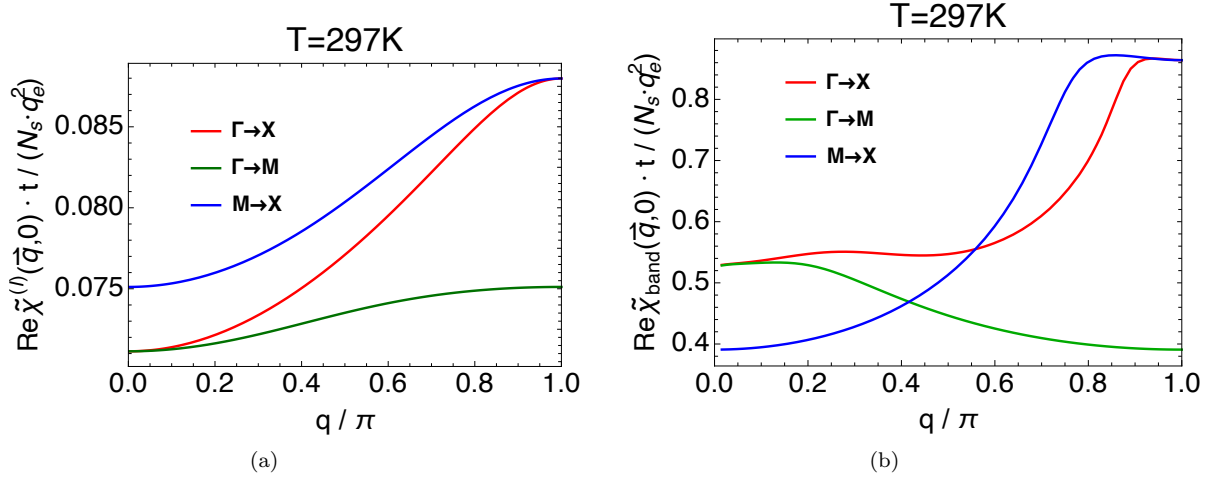


Figure 4: (a) The wave vector dependence of (a) the ECFL static susceptibility $\tilde{\chi}^{(I)}(\vec{q}, 0)$ (Eq. (69)), for different paths in the BZ and (b) the (noninteracting) band structure case (Eq. (44)). The density $n = 0.85$ and q is the relevant component of \vec{q} connecting the (high symmetry) points $\Gamma = (0, 0)$, $X = (\pi, \pi)$, $M = (\pi, 0)$ in the 2-d square lattice BZ.

function $\varphi(\vec{q}, \omega)$ from the complex susceptibility $\tilde{\chi}_{\rho\rho}(\vec{q}, \omega)$ as

$$\varphi(\vec{q}, \omega) = \frac{1}{\tilde{\chi}_{\rho\rho}(\vec{q}, 0)} \left[\frac{\text{Im} \tilde{\chi}_{\rho\rho}(\vec{q}, \omega)}{\pi\omega} \right]. \quad (78)$$

Using a dispersion relation for $\tilde{\chi}_{\rho\rho}(\vec{q}, \omega)$ Eq. (F.7), we verify the normalization condition

$$\int_{-\infty}^{\infty} d\omega \varphi(\vec{q}, \omega) = 1, \quad (79)$$

and also the even-ness $\varphi(\vec{q}, -\omega) = \varphi(\vec{q}, \omega)$. The second frequency moment of this spectral-shape function is given by

$$\int_{-\infty}^{\infty} d\omega \omega^2 \varphi(\vec{q}, \omega) = \Omega_p^2(\vec{q}), \quad (80)$$

where we used Eq. (F.8, F.7, F.10, 58) to relate the result of the integration to the expression in Eq. (59). Thus $\Omega_p(\vec{q})$ provides a characterization of the dynamics of $\tilde{\chi}_{\rho\rho}(\vec{q}, \omega)$. As noted above, our theory identifies this energy as the peak frequency, or equivalently the turn-around scale for $\text{Im} \tilde{\chi}_{\rho\rho}(\vec{q}, \omega)$. In Fig. (20, 21) we plot this energy scale at $n = 0.85$ and $T = 297\text{K}$.

In experiments a reasonable estimate of $\Omega_p(\vec{q})$ might be obtained by an integration over a *finite* frequency window in Eq. (80), if $\varphi(\vec{q}, \omega)$ falls off rapidly with ω [43]. From Eq. (77, 80, F.20), we see that this energy scale results from a ratio of two diminishing scales, the bandwidth reduction and the compressibility reduction, both due of the Gutzwiller-Hubbard correlations. In Fig. (12) we calculate the important characteristic energy $\Omega(\vec{q}, \omega)$ for both approximations in Eq. (69) and Eq. (70) at optimal density $n = 0.85$ and room temperature $T = 295\text{K}$ in the $\Gamma \rightarrow X$ direction.

5.6 Plasma frequency

In Fig. (13) we display the approximate dielectric functions, computed from Eq. (73, 74) at $n = 0.85$ and $T = 295\text{K}$, in the form of $\text{Im} \frac{1}{\varepsilon(\vec{q}, \omega)}$ (panels (a,c)) and $\text{Re} \varepsilon(\vec{q}, \omega)$ (panels (b,d)). The first of these is directly measured in (inelastic) electron loss type experiments where peaks, if present, signify plasmons. The second is a theoretical curve of a type used to identify plasmons through its zero crossing, and is relevant to certain optical experiments. In panels (a,c) we observe a linear in ω behavior as expected in $\text{Im} \epsilon^{(II)}(\vec{q}, \omega)$ for sufficiently small ω , owing to the quasiparticle contribution in the self-energy. As explained above (see the paragraph following Eq. (69)), $\text{Im} \epsilon^{(I)}(\vec{q}, \omega)$, lacks the quasiparticle behavior at low ω . From panels (b,d) we note that unlike in the RPA calculation [7, 14] for uncorrelated materials,

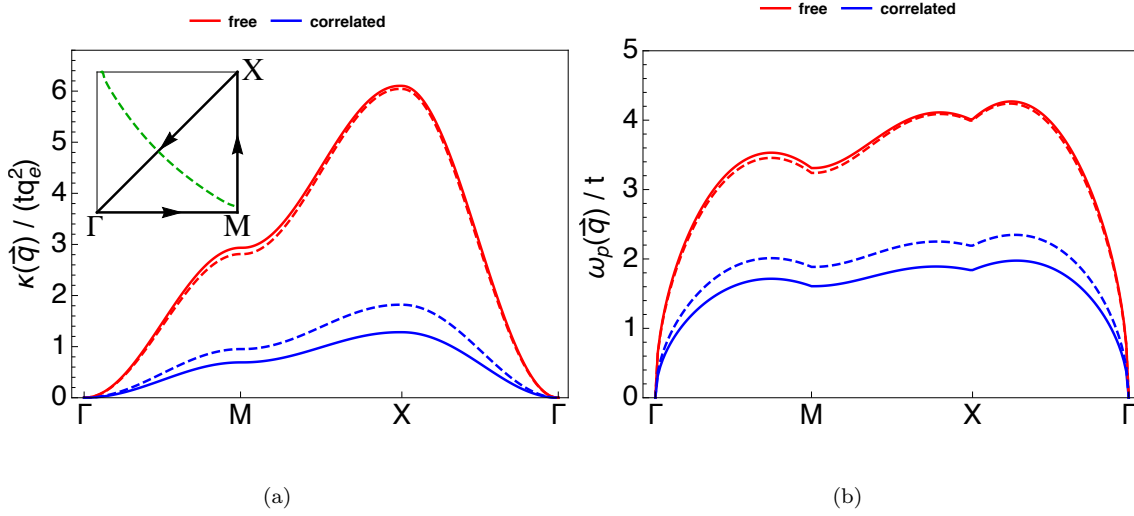


Figure 5: (a) The function $\frac{1}{tq_e^2}\kappa(\vec{q})$ (Eq. (19)) or the first moment $\tilde{\omega}^{(1)}(\vec{q})/t$ (Eq. (F.12)) over the BZ. We used Eq. (F.14), at two densities $n = 0.85$ (solid curves) and $n = 0.8$ (dashed curves) for the uncorrelated (red) and correlated (blue) systems at $T = 297\text{K}$. Recall from Eq. (F.10, F.12), that $\tilde{\omega}^{(1)}(\vec{q})$ can in principle be inferred from experiments. (b) The plasmon dispersion $\omega_p(\vec{q})$ in 2-d from Eq. (E.12, E.7, 7) for the same parameters, and $\varepsilon_\infty = 4.5$, for the uncorrelated (red) and correlated (blue) systems.

$\text{Re}\{\varepsilon\}$ crosses the zero line only for large g_c . In Fig. (14, 15), we focus on the evolution of the $\varepsilon^{(I)}$ over the ranges $q = \pi/16, \pi/8, 3\pi/16$ and $g_c = 10, 50, 100$ in the two principle directions $\Gamma \rightarrow X$ and $\Gamma \rightarrow M$. In Fig. (16) we show the reducible susceptibility $V_{\vec{q}} \text{Im} \chi_{\rho\rho} = -\text{Im}\{1/\varepsilon\}$, obtained using $\tilde{\chi}^{(I)}$ in Eq. (31), for the same set of parameters. It should be noted that $\text{Im} \chi_{\rho\rho}$ is the most directly accessible (i.e. raw) object in inelastic electron scattering experiments, as noted in Eq. (B.6). In Fig. (16), a decrease in magnitude of the peak as $q \rightarrow 0$ is the consequence of the conservation of charge $\lim_{q \rightarrow 0} \rho_q$. We also observe that when g_c is large, the peaks in $\text{Im} \chi_{\rho\rho}$ are broadened out considerably and pushed out to higher energies, as compared to smaller g_c .

5.7 Comparison of $\text{Im} \tilde{\chi}_{\rho\rho}$, $\text{Re} \bar{\sigma}$ and $\text{Im} \tilde{\chi}_{JJ}$

The variable $\text{Re} \bar{\sigma}(\vec{q}, \omega)$ is related to the physical (i.e. dimensional) conductivity through $\text{Re} \sigma(\vec{q}, \omega) = \frac{\hbar}{q_e^2 c_0} \text{Re} \bar{\sigma}(\vec{q}, \omega)$ (see Eq. (E.17)), where c_0 is the separation between two copper oxygen planes in the cuprates. Let us first note the relationships between the three sets of variables $\text{Re} \bar{\sigma}(\vec{q}, \omega)$, $\text{Im} \tilde{\chi}_{JJ}(\vec{q}, \omega)$ and $\text{Im} \tilde{\chi}_{\rho\rho}(\vec{q}, \omega)$. Combining Eq. (E.14, 39) we find

$$\text{For } |\vec{q}|a_0 \ll 1, \text{Im} \tilde{\chi}_{JJ}(\vec{q}, \omega) = \frac{\omega^2}{|\vec{q}|^2} \text{Im} \tilde{\chi}_{\rho\rho}(\vec{q}, \omega), \quad (81)$$

which is a form of the charge conservation law. Combining further with Eq. (E.17)) we get the important relation valid in the regime $|\vec{q}|a_0 \ll 1$:

$$\text{Re} \bar{\sigma}(\vec{q}, \omega) = \frac{1}{\omega} \left(\frac{\text{Im} \tilde{\chi}_{JJ}(\vec{q}, \omega)}{q_e^2 N_s} \right) = \frac{\omega}{|\vec{q}|^2} \left(\frac{\text{Im} \tilde{\chi}_{\rho\rho}(\vec{q}, \omega)}{q_e^2 N_s} \right). \quad (82)$$

In Fig. (17, 18, 19) we display the above closely related triad of variables at room temperature $T = 297, 177, 62\text{K}$ for two density $n = 0.80$ and $n = 0.85$. In panels (a,d) we show the imaginary part of the density susceptibility $\text{Im} \tilde{\chi}_{\rho\rho}(\vec{q}, \omega)$, in panels (b,e) the real part of dimensionless conductivity $\text{Re} \bar{\sigma}(\vec{q}, \omega)$ and in panels (c,f) the current-current susceptibility $\text{Im} \tilde{\chi}_{JJ}(\vec{q}, \omega)$. We compute this objects using our largest systems of $L_x \times L_y = 128 \times 128$, allowing us to access the long wavelength modes $\vec{q} = (\pi/64, \pi/64)$ of the susceptibility.

The overall factor of ω occurs at different locations in the expressions for the three displayed variables, and might be expected to lead to different sensitivity to low frequency noise of various kinds (on an

absolute scale). The variable $\text{Im} \tilde{\chi}_{\rho\rho}$ is most sensitive in this regard. We also note that the peak frequency Ω_p is visible in all three variables, although the peak frequency is slightly different due to a small rightward shift caused by each multiplying factor of ω .

We believe that a systematic study of the variable $\text{Re} \bar{\sigma}(\vec{q}, \omega)$ offers some advantages. It can be obtained from the scattering intensity (via $\text{Im} \tilde{\chi}_{\rho\rho}$), using various available relations. As noted above it might be more stable than $\text{Im} \tilde{\chi}_{\rho\rho}$ against low ω noise. Secondly its low \vec{q} behavior must evolve continuously from the independently measurable optical conductivity at $\vec{q} = 0$, as well as transport measurements at $\omega = 0$. These constraints are expected to be helpful in estimating the absolute scale of the susceptibility [42]. Therefore the systematic study of the deduced $\text{Re} \bar{\sigma}(\vec{q}, \omega)$, together with the optical conductivity $\text{Re} \bar{\sigma}(0, \omega)$ could be most helpful.

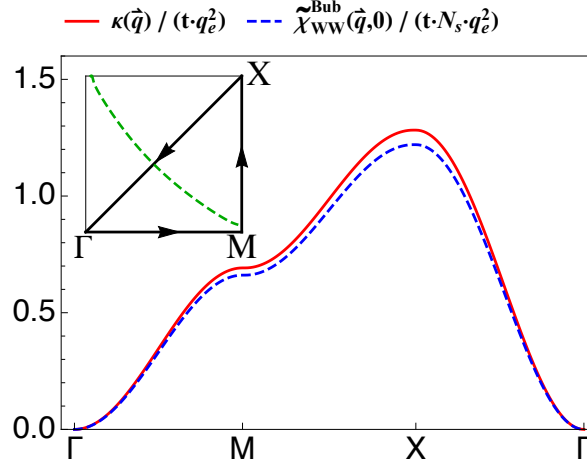


Figure 6: The dimensionless functions $\frac{1}{t q_e^2} \kappa(\vec{q})$ from Eq. (19) and $\frac{1}{t q_e^2 N_s} \tilde{\chi}_{WW}^{\text{Bub}}(\vec{q}, 0)$ from Eq. (62) plotted over the Brillouin zone are approximately identical for a system at $n = 0.85$ and $T = 297\text{K}$. These two curves should coincide identically in an exact calculation of the susceptibility that goes beyond the bubble approximation. The ratio between the two curves in Eq. (65) corrects for this discrepancy.

6 Conclusions and Discussion

We have presented results from our calculation of the dynamics of electron fluctuations in the t - J - V_C model of Eq. (2). We see that the small quasiparticle weight in the normal state gives rise to a broad background in the electron spectral weight Fig. (1). This in turn leads to a smearing of sharp features in the dynamical correlations, as we see in Fig. (9). The small Z also reflects in the flattening of the momentum distribution, as seen in Fig. (2).

The plasmon energy $\omega_p(\vec{q})$ can be extracted in several distinct ways. We have discussed two methods already, from the peaks in $-\text{Im}(\frac{1}{\varepsilon(\vec{q}, \omega)})$, or from the zeroes of $\text{Re} \varepsilon(\vec{q}, \omega)$ as seen in Fig. (13, 14). There is yet another possibility, namely from a measurement of the first frequency moment of the structure function $S(\vec{q}, \omega)$ as in Eq. (F.10, F.12). Here the frequency integration must be large enough to contain all the weight from the primary band containing the Fermi level, but small enough to exclude interband effects. This balance is familiar from studies of optical conductivity in cuprates [40], where satisfying the various versions of the f -sumrule involves parallel issues.

The results for $\text{Im} \tilde{\chi}_{\rho\rho}(\vec{q}, \omega)$ presented in Fig. (10, 11) display a slow fall off for $\omega > \Omega_p$ over a substantial range. This behaviour is similar to the fall off seen experimentally [14, 15]. From Eq. (82) this implies that the current susceptibility $\text{Im} \tilde{\chi}_{JJ}(\vec{q}, \omega)$ should flatten out in the same ω range. This is indeed seen in Fig. (17, 19) in panels (a,c). We should note that in the panels (b,d) of this figure, the conductivity shows a related sluggish fall off with ω , consistent with Eq. (82).

In the region $|\omega| \leq \Omega_p(\vec{q})$, our calculations show that the quasiparticle contribution to $\text{Im} \tilde{\chi}_{\rho\rho}(\vec{q}, \omega)$ leads to a linear in ω behavior, as seen in the contrast between the two plots in Fig. (9), and in all the low \vec{q} plots of in Fig. (10, 11). A low magnitude of Z , as in the ECFL theory makes the linear regime

small, but remain non-zero, and hence worth looking for in data.

Finally we believe that extracting systematically the energy scale $\Omega_p(\vec{q})$ for a range of small \vec{q} values is an important task for future experimental studies. In addition to tracking the peaks of the imaginary parts of the various susceptibilities noted in Eq. (82), as well as Fig. (17) and related figures, approximately evaluating the formula Eq. (80, F.20) using data could provide a useful alternative. It is possibly a difficult task if the $\Omega_p(\vec{q})$ is not sufficiently larger than the experimental resolution, and if other sources such as phonons contribute strongly to the scattering intensity. Such a study would provide insight into the nature of the metallic state in the cuprates.

7 Acknowledgements:

We thank P. Abbamonte for a helpful communication. The work at UCSC was supported by the US Department of Energy (DOE), Office of Science, Basic Energy Sciences (BES), under Award No. DE-FG02-06ER46319. The computation was done on the comet in XSEDE [44] (TG-DMR170044) supported by National Science Foundation grant number ACI-1053575.

A Summary of ECFL Green's function \mathcal{G}

The $\mathcal{O}(\lambda^2)$ approximation of the ECFL equations determining the Green's function for the t - J model has been discussed earlier in our papers Ref. [18, 20, 21], so we provide a very short summary of the equations used. In the ECFL theory, the one-electron Green's function \mathcal{G} is found using the Schwinger method [18], and expressed as a product of an auxiliary Green's function \mathbf{g} and a "caparison" function $\tilde{\mu}$:

$$\mathcal{G}(k) = \mathbf{g}(k) \times \tilde{\mu}(k) \quad (\text{A.1})$$

where $k \equiv (\vec{k}, i\omega_k)$, and $\omega_k = (2k+1)\pi k_B T$ is the Fermionic Matsubara frequency and subscript k is an integer. The auxiliary $\mathbf{g}(k)$ is a Fermi-liquid type Green's function. The Schwinger equation of motion for the physical Green's function can be symbolically written as [18, 20, 21]

$$\left(\mathbf{g}_0^{-1} - \lambda \hat{X} - \lambda Y_1 \right) \cdot \mathcal{G} = \delta (1 - \lambda \gamma). \quad (\text{A.2})$$

where \hat{X} represents a functional derivative and Y_1 describes a Hartree-type energy. Here λ is an expansion parameter and set equal to unity after retaining all second order terms. The non-canonical nature of the Gutzwiller projected operators leads to the term $(1 - \lambda \gamma)$ on the right hand side, this would be just $\mathbf{1}$ for canonical electrons. The decomposition in Eq. (A.1) circumvents this problem since \mathbf{g} is constructed so as to satisfy a canonical equation [18].

To second order (in λ) the ECFL equations [20, 21] are found to be

$$\tilde{\mu}(k) = 1 - \lambda \frac{n}{2} + \lambda \psi(k) \quad (\text{A.3})$$

$$\mathbf{g}^{-1}(k) = i\omega_k + \boldsymbol{\mu} - \epsilon_{\vec{k}} + \lambda \frac{n}{2} \epsilon_{\vec{k}} - \lambda \phi(k) \quad (\text{A.4})$$

where $\boldsymbol{\mu}$ is the chemical potential and $\epsilon_{\vec{k}}$ is the bare band energy Eq. (F.13) and $\psi(k)$ is the second self-energy. The self-energy $\phi(k)$ factors out as $\phi(k) = \chi(k) + \epsilon'_{\vec{k}} \psi(k)$ where $\chi(k)$ is another function defined below, $\epsilon'_{\vec{k}} = \epsilon_{\vec{k}} - u_0/2$, where u_0 is a Lagrange multiplier. Both $\boldsymbol{\mu}$ and u_0 are determined by constraining the number of electrons defined respectively using \mathcal{G} and \mathbf{g} on Eq. (A.10). The two self-energies functions ψ and χ expanded formally in λ to second order approximation $\mathcal{O}(\lambda^2)$ are $\psi = \psi_{[0]} + \lambda \psi_{[1]} + \dots$ and $\chi = \chi_{[0]} + \lambda \chi_{[1]} + \dots$. The expression for these self-energies in the expansion are

$$\psi_{[0]}(k) = 0, \quad \chi_{[0]}(k) = - \sum_p \left(\epsilon'_{\vec{p}} + \frac{1}{2} J_{\vec{k}-\vec{p}} \right) \mathbf{g}(p) \quad (\text{A.5})$$

and

$$\psi_{[1]}(k) = - \sum_{pq} \left(\epsilon'_{\vec{p}} + \epsilon'_{\vec{q}} + J_{\vec{k}-\vec{p}} \right) \mathbf{g}(p) \mathbf{g}(q) \mathbf{g}(p+q-k) \quad (\text{A.6})$$

$$\begin{aligned} \chi_{[1]}(k) = & - \sum_{pq} \left(\epsilon'_{\vec{p}} + \epsilon'_{\vec{q}} + J_{\vec{k}-\vec{q}} \right) \left(\epsilon'_{\vec{p}+\vec{q}-\vec{k}} + J_{\vec{k}-\vec{p}} \right) \\ & \times \mathbf{g}(p) \mathbf{g}(q) \mathbf{g}(p+q-k) \end{aligned} \quad (\text{A.7})$$

where we denote $\sum_k \equiv \frac{k_B T}{N_s} \sum_{\vec{k}, \omega_k}$ and $J_{\vec{q}}$ is the Fourier transform of J_{ij} . With $\lambda \rightarrow 1$, the expressions for the $\mathcal{O}(\lambda^2)$ ECFL equations are

$$\tilde{\mu}(k) = 1 - \frac{n}{2} + \psi(k) \quad (\text{A.8})$$

$$\mathbf{g}^{-1}(k) = i\omega_k + \boldsymbol{\mu} - \epsilon_{\vec{k}} + \frac{n}{2} \epsilon_{\vec{k}} - \chi_{[0]}(k) - \chi_{[1]}(k) - \epsilon'_{\vec{p}} \psi_{[1]}(k). \quad (\text{A.9})$$

We can determine the two chemical potentials $\boldsymbol{\mu}$ and u_0 by satisfying the following number sum rules

$$\sum_k \mathbf{g}(k) e^{i\omega_k 0^+} = \frac{n}{2} = \sum_k \mathcal{G}(k) e^{i\omega_k 0^+}, \quad (\text{A.10})$$

where n is the particle density. We find the spectral function $A(\vec{k}, \omega) = -1/\pi \text{Im} \mathcal{G}(k)$ by analytically continuing (i.e., $i\omega_k \rightarrow \omega + i\eta$) and by solving Eq. (A.1) and Eq. (A.5–A.10) iteratively. We also note the useful spectral representation expressing \mathcal{G} in terms of A :

$$\mathcal{G}(\vec{k}, i\omega_n) = \int_{-\infty}^{\infty} d\nu \frac{A(k, \nu)}{i\omega_n - \nu}. \quad (\text{A.11})$$

B Susceptibilities and the Structure function

Our focus is on the charge susceptibility and the related structure function, and hence we first summarize some standard results [5–8]. Let us define the susceptibility of any pair of operators A, B as

$$\chi_{AB}(\omega + i\eta) = i \int_0^{\infty} dt e^{i\omega t - \eta t} \langle [A(t), B(0)] \rangle \quad (\text{B.1})$$

where $\eta = 0^+$ is a positive infinitesimal, $A(t) = e^{iHt} A e^{-iHt}$, and the brackets denote the usual thermal average. Its causal nature allows us to write a spectral representation

$$\chi_{AB}(\omega + i\eta) = -\frac{1}{\pi} \int_{-\infty}^{\infty} d\nu \frac{\chi''_{AB}(\nu)}{\omega - \nu + i\eta}. \quad (\text{B.2})$$

By integration over t we find the usual expression for the structure function

$$S_{AB}(\omega) = \int_{-\infty}^{\infty} \frac{dt}{2\pi} e^{i\omega t} \langle A(t) B(0) \rangle, \quad (\text{B.3})$$

and

$$S_{AB}(\omega) = \frac{1}{\pi} \frac{\chi''_{AB}(\omega)}{1 - e^{-\beta\omega}}. \quad (\text{B.4})$$

In order to obtain the charge density structure function $S_{\rho\rho}(\vec{q}, \omega)$, we must calculate the charge susceptibility $\chi_{\rho\rho}$ defined from Eq. (B.1) as

$$A = \rho_q = q_e \sum_{k\sigma} \tilde{C}_{k\sigma}^\dagger \tilde{C}_{k+q\sigma}, \quad \text{and} \quad B = \rho_{-q} = A^\dagger, \quad (\text{B.5})$$

where $q_e = -|e|$ is the electron charge. $S_{\rho\rho}(\vec{q}, \omega)$ is a very important object since it is obtained directly from experimentally determined electron scattering intensity, with energy transfer $\hbar\omega$ and momentum transfer $\hbar\vec{q}$. From this object, the reducible susceptibility $\chi''_{\rho\rho}(\vec{q}, \omega)$ can be obtained using the fact that it is an odd function of ω . Hence

$$\chi''_{\rho\rho}(\vec{q}, \omega) = \pi (S_{\rho\rho}(\vec{q}, \omega) - S_{\rho\rho}(\vec{q}, -\omega)). \quad (\text{B.6})$$

In real space we write the local charge density ρ_m at site m as

$$\rho_m \equiv q_e n_m, \quad \text{and} \quad \rho_m = \frac{1}{N_s} \sum_q e^{i\vec{q} \cdot \vec{r}_m} \rho_q, \quad (\text{B.7})$$

where N_s is the number of lattice sites. For our calculations it is more convenient to evaluate the imaginary time object and its Fourier transform

$$\chi_{AB}(\tau) = \langle T_\tau A(\tau) B(0) \rangle, \quad \text{and} \quad \chi_{AB}(i\Omega_\nu) = \frac{1}{2} \int_{-\beta}^{\beta} d\tau e^{i\Omega_\nu \tau} \chi_{AB}(\tau), \quad (\text{B.8})$$

where $\Omega_\nu = \frac{2\pi}{\beta} \nu$ and $\nu = 0, \pm 1, \pm 2, \dots$. We can use analytic continuation $i\Omega_\nu \rightarrow \omega + i0^+$ to obtain the physical susceptibility $\chi_{AB}(\omega + i\eta)$ Eq. (B.1) from Eq. (B.8).

C Reducible susceptibility χ from \mathcal{G}

We next turn to calculation of the susceptibilities from the electronic Green's functions. For this purpose we need to calculate the Green's functions in the presence of external potentials, and taking the derivatives we can find the susceptibilities. Although this procedure might be familiar to most readers, we summarize the steps below for completeness. In order to calculate the Green's functions for this model, we add an imaginary time τ dependent external potential (or source term) \mathcal{A} to the definition of thermal averages. The expectation of an arbitrary observable $Q(\tau_1, \dots)$, composed e.g. of a product of several (imaginary) time ordered Heisenberg picture operators, is written in the notation

$$\langle\langle Q(\tau_1, \dots) \rangle\rangle = \text{Tr } P_\beta T_\tau \{e^{-\mathcal{A}} Q(\tau_1, \dots)\}. \quad (\text{C.1})$$

Here T_τ is the time-ordering operator, an external potential term $\mathcal{A} = \int_0^\beta d\tau \mathcal{A}(\tau)$, and $P_\beta = e^{-\beta H} / \text{Tr} (e^{-\beta H} T_\tau e^{-\mathcal{A}})$ is the Boltzmann weight factor including \mathcal{A} . Here $\mathcal{A}(\tau)$ is a sum of two terms, $\mathcal{A}_V(\tau)$ involving a density-spin dependent external potential \mathcal{V} , and $\mathcal{A}_{uv}(\tau)$ involving external potentials $u_m(\tau), v_m(\tau)$ coupling to the charge and the W variables of Eq. (9, 10). These are given by

$$\begin{aligned} \mathcal{A}_V(\tau) &= \sum_i \mathcal{V}_i^{\sigma_i \sigma_j}(\tau) \tilde{C}_{i\sigma_i}^\dagger(\tau) \tilde{C}_{i\sigma_j}(\tau) \\ \mathcal{A}_{uv}(\tau) &= \sum_m (u_m(\tau) \rho_m(\tau) + v_m(\tau) W_m(\tau)). \end{aligned} \quad (\text{C.2})$$

At the end of the calculations, the external potentials \mathcal{V}, u, v are switched off, so that the average in Eq. (C.1) reduces to the standard thermal average. We can find the equation of motion for the electron Green's function

$$\mathcal{G}_{i\sigma_i j\sigma_j}(\tau, \tau') = -\langle\langle \tilde{C}_{i\sigma_i}(\tau) \tilde{C}_{j\sigma_j}^\dagger(\tau') \rangle\rangle \quad (\text{C.3})$$

by standard methods described in literature. In particular by using the identity valid for any operator Q and external potential taken to be v_i for illustration:

$$\text{Tr } P_\beta T_\tau \{e^{-\mathcal{A}} Q_i(\tau') W_j(\tau)\} = \langle\langle Q_i(\tau') \rangle\rangle \langle\langle W_j(\tau) \rangle\rangle - \frac{\delta}{\delta v_i(\tau)} \langle\langle Q_i(\tau') \rangle\rangle \quad (\text{C.4})$$

we can reduce higher order Green's functions to functional derivatives of the lower order ones. A straightforward calculation using the method described in [18] gives the exact functional differential equation satisfied by \mathcal{G} . Let us define

$$\begin{aligned} \gamma_{\sigma_i \sigma_j}(i, \tau) &= \sigma_i \sigma_j \langle\langle \tilde{C}_{i\sigma_i}^\dagger(\tau) \tilde{C}_{i\sigma_j}(\tau) \rangle\rangle \\ \mathcal{D}_{\sigma_i \sigma_j}(i, \tau) &= \sigma_i \sigma_j \frac{\delta}{\delta \mathcal{V}_i^{\sigma_i \sigma_j}(\tau)}, \end{aligned} \quad (\text{C.5})$$

the non-interacting Green's function G_0 including all the external potentials:

$$\begin{aligned} G_{0i\sigma_i j\sigma_j}^{-1} &= \delta_{ij} \delta_{\sigma_i \sigma_j} (\boldsymbol{\mu} - \partial_{\tau_i}) + t_{ij} \delta_{\sigma_i \sigma_j} - \delta_{ij} \mathcal{V}_i^{\sigma_i \sigma_j} \\ &\quad - q_e u_i \delta_{ij} - i q_e (v_i - v_j) t_{ij}, \end{aligned} \quad (\text{C.6})$$

the standard Hartree type Y variables from [18]

$$\begin{aligned} Y_{i\sigma_i j\sigma_j} &= t_{ij} \gamma_{\sigma_i \sigma_j}(i, \tau_i) - \delta_{ij} \frac{1}{2} \sum_k J_{ik} \gamma_{\sigma_i \sigma_j}(k, \tau_i) \\ &\quad + \delta_{ij} \sum_l V_{il} \langle\langle n_l(\tau_i) \rangle\rangle \end{aligned} \quad (\text{C.7})$$

and the X type functional derivative terms

$$\begin{aligned} X_{i\sigma_i j\sigma_j} &= -t_{ij} \mathcal{D}_{\sigma_i \sigma_j}(i) + \delta_{ij} \frac{1}{2} \sum_k J_{ik} \mathcal{D}_{\sigma_i \sigma_j}(k, \tau_i) \\ &\quad - q_e \delta_{ij} \sum_l V_{il} \frac{\delta}{\delta u_l(\tau_i)}. \end{aligned} \quad (\text{C.8})$$

In the equations Eq. (C.6, C.7, C.8) a factor of $\delta(\tau_i - \tau_j)$ right-multiplying all the terms has been suppressed for brevity. We find the exact equation for \mathcal{G} in a compact form by using a repeated spin index summation notation as:

$$\begin{aligned} (G_{0i\sigma_i j\sigma_j}^{-1} - Y_{i\sigma_i j\sigma_j} - X_{i\sigma_i j\sigma_j}) \mathcal{G}_{j\sigma_j f\sigma_f}(\tau_i, \tau_f) \\ = \delta(\tau_i - \tau_f) \delta_{if} (\delta_{\sigma_i \sigma_f} - \gamma_{\sigma_i \sigma_f}(i, \tau_i)). \end{aligned} \quad (\text{C.9})$$

The expressions for Y in Eq. (C.7) and X in Eq. (C.8) reduce to the corresponding equations for the pure t - J model in [20, 21], if we drop the Coulomb terms in the last lines, i.e. $V_{il} \rightarrow 0$, and also drop the source terms with u and v in the last line of Eq. (C.6). Following standard practice for Coulomb interactions [5], an implicit neutralizing background term cancels the divergence of the $q = 0$ component of the last Hartree-type term in Y in Eq. (C.7).

In terms of the Green's function, the expectation value of the density and the W-variables are found as

$$\langle \langle \rho_m(\tau) \rangle \rangle = \sum_{if\sigma} \gamma_\rho(i, f; m) \mathcal{G}_{\sigma\sigma}(i\tau, f\tau^+) \quad (\text{C.10})$$

$$\langle \langle W_m(\tau) \rangle \rangle = \sum_{if\sigma} \gamma_W(i, f; m) \mathcal{G}_{\sigma\sigma}(i\tau, f\tau^+) \quad (\text{C.11})$$

where we introduced the bare vertices for the charge ρ and the divergence of current W :

$$\begin{aligned} \gamma_\rho(i, f; m) &\equiv q_e \delta_{i,m} \delta_{f,m} = -\frac{\delta}{\delta u_m(\tau)} G_{0i\sigma_i f\sigma_j}^{-1} \\ \gamma_W(i, f; m) &\equiv i q_e t_{if} (\delta_{i,m} - \delta_{f,m}) = -\frac{\delta}{\delta v_m(\tau)} G_{0i\sigma_i f\sigma_j}^{-1}. \end{aligned} \quad (\text{C.12})$$

Using Eq. (C.4) we write down the four relevant susceptibilities in real space:

$$\begin{aligned} \chi_{\rho\rho}(i\tau_i j\tau_j) &= -\frac{\delta}{\delta u_j(\tau_j)} \sum_{lm\sigma} \gamma_\rho(l, m; i) \mathcal{G}_{\sigma\sigma}(l\tau_i, m\tau_i^+) \\ \chi_{WW}(i\tau_i j\tau_j) &= -\frac{\delta}{\delta v_j(\tau_j)} \sum_{lm\sigma} \gamma_W(l, m; i) \mathcal{G}_{\sigma\sigma}(l\tau_i, m\tau_i^+) \\ \chi_{\rho W}(i\tau_i j\tau_j) &= -\frac{\delta}{\delta v_j(\tau_j)} \sum_{lm\sigma} \gamma_\rho(l, m; i) \mathcal{G}_{\sigma\sigma}(l\tau_i, m\tau_i^+) \\ \chi_{W\rho}(i\tau_i j\tau_j) &= -\frac{\delta}{\delta u_j(\tau_j)} \sum_{lm\sigma} \gamma_W(l, m; i) \mathcal{G}_{\sigma\sigma}(l\tau_i, m\tau_i^+) \end{aligned} \quad (\text{C.13})$$

To compress the notation we introduce Greek symbols μ, ν taking two values, with $\mu = \{\rho, W\}$, with ρ denoting charge and W denoting the W-variable (divergence of current). The two bare vertices γ_ρ and γ_W in Eq. (C.12) can now be represented by γ_μ , and the external potentials by w_μ with $w_\rho(i\tau_i) = u_i(\tau_i)$ and $w_W(i\tau_i) = v_i(\tau_i)$. The four relations in Eq. (C.13) can then be compactly written as

$$\chi_{\mu\nu}(i\tau_i j\tau_j) = -\frac{\delta}{\delta w_\nu(j\tau_j)} \sum_{lm\sigma} \gamma_\mu(l, m; i) \mathcal{G}_{\sigma\sigma}(l\tau_i, m\tau_i^+). \quad (\text{C.14})$$

D Irreducible susceptibility $\tilde{\chi}$ from \mathcal{G}

In order to treat the most important effect of long-ranged Coulomb interactions, we must first account for screening. In the case of the electron gas this is achieved by introducing screened vertices and their Feynman diagram definitions in the enlightening discussion in Nozières book [5] and useful summaries in [9, 10]. The projected electrons lack Feynman diagrams and require an alternate treatment. More fundamentally the non canonical nature of the projected electrons creates an obstacle for defining reasonable vertex operators [18], which tend to free vertices at high frequencies. This situation prevents us from borrowing Nozières treatment of screening, and an adaptation is necessary. For this purpose a more general discussion is provided here, working directly with the susceptibilities instead of the vertices.

The main qualitative idea behind our treatment of screening, is to eliminate the long-ranged Hartree-type Coulomb term in the self energy Y appearing on the last line of Eq. (C.7). This term is absorbed

into the redefined external potential term $q_e \tilde{u}_i$ in the non-interacting Green's function Eq. (C.6). We define a screened external potential

$$q_e \tilde{u}_i(\tau) = q_e u_i(\tau) + \sum_l V_{il} \langle \langle n_l(\tau) \rangle \rangle. \quad (\text{D.1})$$

The Green's function is unchanged since we merely shifted the location of the Hartree-type term in Eq. (C.9). We may now regard the Green's function as a functional of \tilde{u}_i rather than u_i . With this modification, we can use a chain rule for taking derivatives

$$\begin{aligned} \frac{\delta}{\delta u_i(\tau_i)} &= \frac{\delta}{\delta \tilde{u}_i(\tau_i)} + \sum_j \int_0^\beta d\tau_j \frac{\delta \tilde{u}_j(\tau_j)}{\delta u_i(\tau_i)} \frac{\delta}{\delta \tilde{u}_j(\tau_j)} \\ &= \frac{\delta}{\delta \tilde{u}_i(\tau_i)} - \frac{1}{q_e^2} \sum_j \int_0^\beta d\tau_j V_{ij} \chi_{\rho\rho}(j\tau_j, i\tau_i) \frac{\delta}{\delta \tilde{u}_j(\tau_j)}. \end{aligned} \quad (\text{D.2})$$

Here the partial derivative $\frac{\delta}{\delta \tilde{u}_j(\tau_j)}$ is taken at fixed values of \tilde{u}_i , where $i \neq j$.

In order to take the derivatives $\frac{\delta}{\delta v_i}$ in Eq. (C.13), we should note that a variation of v_i also induces a variation in \tilde{u}_i , which depend on it through the second term in Eq. (D.1). We can account for this dependence by defining a screened set of potentials $\{\tilde{v}_j\}$, which are independent of \tilde{u}_i .

The derivatives with respect to v_i are relatable to the derivatives with respect to \tilde{v}_i and \tilde{u}_i through the chain rule:

$$\begin{aligned} \frac{\delta}{\delta v_i(\tau_i)} &= \frac{\delta}{\delta \tilde{v}_i(\tau_i)} + \sum_j \int_0^\beta d\tau_j \frac{\delta \tilde{u}_j(\tau_j)}{\delta v_i(\tau_i)} \frac{\delta}{\delta \tilde{u}_j(\tau_j)} \\ &= \frac{\delta}{\delta \tilde{v}_i(\tau_i)} - \frac{1}{q_e^2} \sum_j \int_0^\beta d\tau_j V_{ij} \chi_{\rho W}(j\tau_j, i\tau_i) \frac{\delta}{\delta \tilde{u}_j(\tau_j)}. \end{aligned} \quad (\text{D.3})$$

The second term captures the non-local variation of the \tilde{u}_j by changing v_i that is evident in Eq. (D.1). Therefore for computing the susceptibilities in Eq. (C.13) and Eq. (C.14), we can replace the derivatives with respect to the independent sets of external potentials $\{u_j, v_j\}$ by another independent set of potentials $\{\tilde{u}_j, \tilde{v}_j\}$ related by Eq. (D.3).

Combining Eq. (D.2) and Eq. (D.3) we write

$$\frac{\delta}{\delta w_\nu(i\tau_i)} = \frac{\delta}{\delta \tilde{w}_\nu(i\tau_i)} - \frac{1}{q_e^2} \sum_j \int_0^\beta d\tau_j V_{ij} \chi_{\rho\nu}(j\tau_j, i\tau_i) \frac{\delta}{\delta \tilde{u}_j(\tau_j)}. \quad (\text{D.4})$$

To summarize the above discussion, the Green's functions of the theory, while Eq. (C.9) is unchanged, Eq. (C.6, C.7, C.8) are now functionals of the variables \tilde{u}_i, \tilde{v}_i ,

$$\begin{aligned} G_{0i\sigma_i j\sigma_j}^{-1} &= \delta_{ij} \delta_{\sigma_i \sigma_j} (\boldsymbol{\mu} - \partial_{\tau_i}) + t_{ij} \delta_{\sigma_i \sigma_j} - \delta_{ij} \mathcal{V}_i^{\sigma_i \sigma_j} \\ &\quad - q_e \tilde{u}_i - i q_e (\tilde{v}_i - \tilde{v}_j) t_{ij}, \end{aligned} \quad (\text{D.5})$$

$$\begin{aligned} Y_{i\sigma_i j\sigma_j} &= t_{ij} \gamma_{\sigma_i \sigma_j}(i\tau_i) - \delta_{ij} \frac{1}{2} \sum_k J_{ik} \gamma_{\sigma_i \sigma_j}(k\tau_i) \\ X_{i\sigma_i j\sigma_j} &= -t_{ij} \mathcal{D}_{\sigma_i \sigma_j}(i) + \delta_{ij} \frac{1}{2} \sum_k J_{ik} \mathcal{D}_{\sigma_i \sigma_j}(k\tau_i) \\ &\quad - q_e \delta_{ij} \sum_l V_{il} \frac{\delta}{\delta u_l(\tau_i)}, \end{aligned} \quad (\text{D.6})$$

where the derivative $\frac{\delta}{\delta u_l(\tau_i)}$ in the last term, can be eliminated using Eq. (D.2). The Hartree type approximations made below throws out this last term completely, and hence we skip the details.

We now denote the set of four screened susceptibilities $\tilde{\chi}_{\mu\nu}$ in the form of Eq. (C.14)

$$\tilde{\chi}_{\mu\nu}(i\tau_i, j\tau_j) = -\frac{\delta}{\delta \tilde{w}_\nu(j\tau_j)} \sum_{lm\sigma} \gamma_\mu(l, m; i) \mathcal{G}_{\sigma\sigma}(l\tau_i, m\tau_i^+) \quad (\text{D.7})$$

where \tilde{w}_μ is either \tilde{u} or \tilde{v} . Using the chain rules Eq. (D.4) we find the important result connecting the unscreened and screened susceptibilities

$$\begin{aligned} \chi_{\mu\nu}(i\tau_i, j\tau_j) &= \tilde{\chi}_{\mu\nu}(i\tau_i, j\tau_j) \\ &- \frac{1}{q_e^2} \sum_m \int_0^\beta d\tau_m V_{im} \tilde{\chi}_{\mu\rho}(i\tau_i, m\tau_m) \chi_{\rho\nu}(m\tau_m, j\tau_j) \end{aligned} \quad (\text{D.8})$$

Upon switching off the external potentials we recover translation invariance, and on taking the Fourier transform of this equation, we find an algebraic equation at each $q \equiv \{\vec{q}, i\Omega\}$

$$\chi_{\mu\nu}(q) = \tilde{\chi}_{\mu\nu}(q) - \frac{1}{q_e^2} V(\vec{q}) \tilde{\chi}_{\mu\rho}(q) \chi_{\rho\nu}(q). \quad (\text{D.9})$$

This can be solved for all the components and displays the screened nature of the resulting susceptibilities. The density-density response $\chi_{\rho\rho}$ is simplest since all terms on the right have the same subscripts. Gathering terms $\chi_{\mu\nu}(q)$ on the left, we find

$$\chi_{\rho\rho}(q) = \frac{\tilde{\chi}_{\rho\rho}(q)}{\varepsilon(q)}, \quad (\text{D.10})$$

where dielectric function is given (exactly) by

$$\varepsilon(q) \equiv \varepsilon(\vec{q}, \omega) = 1 + \frac{1}{q_e^2} V(\vec{q}) \tilde{\chi}_{\rho\rho}(\vec{q}, \omega), \quad (\text{D.11})$$

with the Coulomb potential given by Eq. (6, 7). Proceeding similarly we find the other three susceptibilities in terms of their screened counterparts as

$$\chi_{\rho W}(q) = \frac{\tilde{\chi}_{\rho W}(q)}{\varepsilon(q)}, \quad (\text{D.12})$$

$$\chi_{W\rho}(q) = \frac{\tilde{\chi}_{W\rho}(q)}{\varepsilon(q)}, \quad (\text{D.13})$$

$$\chi_{WW}(q) = \tilde{\chi}_{WW}(q) - \frac{V(\vec{q})}{q_e^2 \varepsilon(q)} \tilde{\chi}_{W\rho}(q) \tilde{\chi}_{\rho W}(q). \quad (\text{D.14})$$

E Low and high ω limits of $\varepsilon(\vec{q}, \omega)$

E.1 Low ω : Static Screening and Compressibility

At low frequencies $\omega \rightarrow 0$ and in the long-wavelength limit $|\vec{q}| \ll 1$, the screened susceptibility $\tilde{\chi}_{\rho\rho}$ defined in Eq. (C.14) equals the thermodynamic derivative

$$\lim_{q \rightarrow 0} \lim_{\omega \rightarrow 0} \tilde{\chi}_{\rho q \rho - q}(\vec{q}, \omega) = q_e^2 \frac{dn}{d\mu} N_s. \quad (\text{E.1})$$

In view of the connection with the compressibility Eq. (E.5), this is often called the *compressibility sum-rule*. To see this we note that a space independent $-q_e \tilde{u}$ is *additive* to the chemical potential μ in Eq. (D.6), and since the nominally divergent Hartree term is removed in defining \tilde{u} the uniform limit is safely taken. This gives the compressibility sum-rule, i.e., the screening limit of the dielectric constant [1, 3, 5]

$$\lim_{q \rightarrow 0} \lim_{\omega \rightarrow 0} \varepsilon(\vec{q}, \omega) = 1 + V(\vec{q}) N_s \frac{dn}{d\mu} \quad (\text{E.2})$$

Thus in 3-d and 2-d we get the exact result:

$$\varepsilon \rightarrow 1 + \frac{q_s^2}{|\vec{q}|^2}, \quad (3\text{-d}) \text{ with } q_s^2 = \frac{4\pi q_e^2}{\varepsilon_\infty} \frac{dn}{d\mu} \quad (\text{E.3})$$

$$\varepsilon \rightarrow 1 + \frac{q_s}{|\vec{q}|}, \quad (2\text{-d}) \text{ with } q_s = \frac{2\pi q_e^2}{\varepsilon_\infty} \frac{dn}{d\mu} \quad (\text{E.4})$$

Using the thermodynamic relation for compressibility χ_{comp}

$$\chi_{comp} = \frac{1}{n^2} \frac{dn}{d\mu}, \quad (\text{E.5})$$

the screening length $\lambda_s = 2\pi/q_s$ can thus be related to the compressibility χ_{comp} .

Strongly correlated systems near half filling display a reduced compressibility, and are therefore expected to show very poor screening, i.e., $\lambda_s \gg 1$ (we set the lattice constant $a_0 = 1$).

E.2 High ω : Plasmon Dispersion in $\varepsilon(q)$

In the limit $\omega \gg t$ the behavior of the dielectric function is easily read off from Eq. (43). Neglecting

$\frac{\tilde{\chi}_{WW}(\vec{q}, \omega)}{\chi_{WW}(\vec{q}, 0)}$ compared to unity, we get

$$\lim_{\omega \gg t} \varepsilon(\vec{q}, \omega) = 1 - \frac{\omega_p^2(\vec{q})}{\omega^2}. \quad (\text{E.6})$$

In both 3-d and 2-d, the plasma frequency is given in terms of κ by

$$\omega_p^2(\vec{q}) = \frac{N_s}{q_e^2} V(\vec{q}) \kappa(\vec{q}). \quad (\text{E.7})$$

In 3-d the plasma frequency can be written using Eq. (19) and Eq. (6) as

$$\omega_p^2(\vec{q}) = \frac{8\pi q_e^2}{\varepsilon_\infty |\vec{q}|^2} \frac{1}{N_s} \sum_{k\sigma} (\varepsilon_{\vec{k}+\vec{q}} - \varepsilon_{\vec{k}}) \langle \tilde{C}_{\vec{k}\sigma}^\dagger \tilde{C}_{\vec{k}+\vec{q}\sigma} \rangle. \quad (\text{E.8})$$

In the long wavelength limit we find

$$\lim_{q \rightarrow 0} \omega_p^2(\vec{q}) = \frac{4\pi q_e^2}{\varepsilon_\infty} \frac{1}{N_s} \sum_{k\sigma} \left(\frac{d^2 \varepsilon_{\vec{k}}}{dk_x^2} \right) \langle \tilde{C}_{\vec{k}\sigma}^\dagger \tilde{C}_{\vec{k}\sigma} \rangle = \frac{4\pi}{\varepsilon_\infty} \mathcal{T}, \quad (\text{E.9})$$

where we used Eq. (21) in the last line. For quadratic dispersion $\varepsilon_k = |\vec{k}|^2/(2m)$, we get the familiar expression $\omega_p^2 = \frac{4\pi n q_e^2}{m \varepsilon_\infty}$. The f-sumrule Eq. (22) is expressible in terms of the plasma frequency as

$$\int_{-\infty}^{\infty} \frac{d\omega}{\pi} \text{Re } \sigma(\omega) = \frac{\varepsilon_\infty}{4\pi} \omega_p^2(0). \quad (\text{E.10})$$

In 2-d using Eq. (19) and Eq. (7) we obtain the acoustic plasmon energy

$$\omega_p^2(\vec{q}) = \frac{4\pi q_e^2}{\varepsilon_\infty |\vec{q}|} \frac{1}{N_s} \sum_{k\sigma} (\varepsilon_{\vec{k}+\vec{q}} - \varepsilon_{\vec{k}}) \langle \tilde{C}_{\vec{k}\sigma}^\dagger \tilde{C}_{\vec{k}+\vec{q}\sigma} \rangle \quad (\text{E.11})$$

$$\lim_{q \rightarrow 0} \omega_p^2(\vec{q}) = |\vec{q}| \times \frac{2\pi q_e^2}{\varepsilon_\infty} \frac{1}{N_s} \sum_{k\sigma} \left(\frac{d^2 \varepsilon_{\vec{k}}}{dk_x^2} \right) \langle \tilde{C}_{\vec{k}\sigma}^\dagger \tilde{C}_{\vec{k}\sigma} \rangle = |\vec{q}| \times \frac{2\pi}{\varepsilon_\infty} \mathcal{T}. \quad (\text{E.12})$$

For quadratic dispersion this reduces to $\omega_p^2 = |\vec{q}| \times \frac{2\pi n q_e^2}{m \varepsilon_\infty}$. This implies that the plasmon mode, found as the zero of the dielectric function is gapless in 2-d with a dispersion $\omega_q \propto \sqrt{q}$, as opposed to the usual gapless mode in 3-d.

Let us note that the effect of Gutzwiller type short range correlations is seen most directly in expressions for \mathcal{T} in Eq. (F.16) and in Fig. (5). We discuss in Section-(F.2) the connection of this result with the first frequency sum rule for the electron structure function.

E.3 The Resistivity Formula:

We note that the formula in Eq. (43) also gives the correct resistivity formula used in studies of the t - J model. Let us first examine the 3-dimensional case with a cubic unit cell, and assume that the electric field polarization is longitudinal, i.e. the current is along \vec{q} . From the usual relation between the induced

current and the polarization $\vec{J}_{ind} = \dot{\vec{P}}$, and $\vec{P} = \frac{1}{4\pi}(\vec{D} - \vec{E})$ combined with the constitutive relations $\vec{J}_{ind} = \sigma \vec{E}$ and $\vec{D} = \varepsilon \vec{E}$ we obtain $\sigma(q) = \frac{\omega}{4\pi i}(\varepsilon(q) - 1)$ and on using Eq. (43)

$$\sigma(\vec{q}, \omega) = \frac{i}{|\vec{q}|^2 \omega} \left(\kappa(q) - \frac{1}{N_s} \tilde{\chi}_{WW}(q) \right). \quad (\text{E.13})$$

In the uniform limit $q \rightarrow 0$ we note from Eq. (12) that $W_q \rightarrow -i\vec{q} \cdot \vec{J}_q$ and $W_{-q} \rightarrow i\vec{q} \cdot \vec{J}_{-q}$; therefore

$$\text{For } |\vec{q}|a_0 \ll 1, \quad \tilde{\chi}_{JJ}(\vec{q}, \omega) = \frac{1}{|\vec{q}|^2} \tilde{\chi}_{WW}(\vec{q}, \omega). \quad (\text{E.14})$$

This is the screened analog of Eq. (16). In the limit $\vec{q} = 0$, there is no distinction between longitudinal and transverse response, and hence using Eq. (21) we get the conductivity accessible in optical experiments

$$\begin{aligned} \sigma(\omega) &= \frac{i}{\omega} \frac{1}{N_s} \left(q_e^2 \sum_{k\sigma} \left(\frac{d^2 \varepsilon_k}{dk_x^2} \right) \langle \tilde{C}_{k\sigma}^\dagger \tilde{C}_{k\sigma} \rangle - \tilde{\chi}_{JJ}(\omega) \right), \\ &= \frac{i}{\omega} \left(\mathcal{T} - \frac{1}{N_s} \tilde{\chi}_{JJ}(\omega) \right) \end{aligned} \quad (\text{E.15})$$

with $\omega \equiv \omega + i0^+$. Let us note an important consequence of Eq. (E.13):

$$\text{Re } \sigma(\vec{q}, \omega) = \frac{1}{\omega N_s} \text{Im } \tilde{\chi}_{JJ}(\vec{q}, \omega), \quad (\text{E.16})$$

thus relating the dissipative part of conductivity with $\text{Im } \tilde{\chi}_{JJ}(\vec{q}, \omega)/\omega$. In Eq. (E.16) we have suppressed an implicit prefactor $\frac{1}{a_0}$, which needs modification for quasi 2-dimensional system such as the cuprate materials analyzed in [21, 31]. Here the theory proceeds by assuming that the unit cell is body centered tetragonal instead of cubic. Here a_0 is replaced by c_0 , the separation between two copper oxide layers in the simple case of single layer cuprates, so that $c_0 \gg a_0$. The different layers are assumed to be decoupled as far as electron hopping is concerned, while their polarizations add up. We then obtain an appropriate generalization of Eq. (E.16)

$$\text{Re } \sigma(\vec{q}, \omega) = \frac{q_e^2}{c_0 h} \left(\frac{h}{q_e^2 \omega N_s} \text{Im } \tilde{\chi}_{JJ}(\vec{q}, \omega) \right), \quad (\text{E.17})$$

where the object in parentheses is $\mathcal{O}(1)$ and dimensionless. We note that Eq. (E.15) is almost identical to the standard formula for the optical conductivity $\sigma(\omega)$ obtained from the Kubo formula for Hubbard model or t - J model type systems without the long ranged Coulomb interaction, e.g. see Eq. (A1-A5) in [32]. The only change is that the screened current susceptibility $\tilde{\chi}_{JJ}$ replaces the unscreened χ_{JJ} . This object can be obtained from Eq. (36) in the limit of small \vec{q} . Physically the tilde means that the calculation of the current-current correlators must discard direct contributions from the Coulomb potential. The f-sumrule for the conductivity $\int_{-\infty}^{\infty} \frac{d\omega}{\pi} \text{Re } \sigma(\omega) = \mathcal{T}$ given in Eq. (22), follows by first writing the Kramers-Kronig relation

$$\text{Im } \sigma(\omega) = \frac{1}{\pi} \int_{-\infty}^{\infty} d\nu \frac{\text{Re } \sigma(\nu)}{\omega - \nu}, \quad (\text{E.18})$$

taking the limit $\omega \gg 0$, and finally comparing the expression with the coefficient of $1/\omega$ in Eq. (E.15).

F Structure Function Frequency Moments

The recent momentum dependent electron energy loss experiments (M-EELS) [13–15] probe charge response inferred from the inelastic momentum resolved scattering of electrons from the surface of the high T_c superconductor $\text{Bi}_{2212} \text{Bi}_2\text{Sr}_2\text{CaCu}_2\text{O}_{8+x}$. Making various simplifying assumptions that are argued for in the work of Mills [39], the experiment gives a readout of the structure function

$$S_{\rho\rho}(\vec{q}, \omega) = \int_{-\infty}^{\infty} \frac{dt}{2\pi} e^{i\omega t} \langle \rho_{\vec{q}}(t) \rho_{-\vec{q}}(0) \rangle = \frac{1}{\pi} \frac{\chi''_{\rho\rho}(\vec{q}, \omega)}{1 - e^{-\beta\omega}}, \quad (\text{F.1})$$

over a substantial portion of the \vec{q}, ω region with remarkably high precision. The energy resolution $\Delta\omega \sim 2\text{meV}$. Here \vec{q} is taken to be 2-dimensional. These works present direct information about $\chi_{\rho\rho}$, in fact using the odd-ness of $\chi''_{\rho\rho}$ we can extract this object by combining energy loss and energy gain data:

$$\chi''_{\rho\rho}(\vec{q}, \omega) = \pi (S_{\rho\rho}(\vec{q}, \omega) - S_{\rho\rho}(\vec{q}, -\omega)) \quad (\text{F.2})$$

The work of [13–15] presents data for the $\chi''_{\rho\rho}(\omega)$ as well as the inferred screened susceptibility $\tilde{\chi}_{\rho\rho}$.

F.1 High frequency moments: reducible susceptibility

Using the familiar analyticity of $\chi_{\rho\rho}(\vec{q}, \omega)$ in the upper half of the complex ω plane, we can write a spectral representation

$$\chi_{\rho\rho}(\vec{q}, \omega) = -\frac{1}{\pi} \int_{-\infty}^{\infty} d\nu \frac{\chi_{\rho\rho}''(\vec{q}, \nu)}{\omega - \nu + i0^+}. \quad (\text{F.3})$$

We note that $\chi_{\rho\rho}''(\vec{q}, \nu)$ is odd in ω and hence as $\omega \gg 0$ we get a moment expansion with even terms [41]

$$\lim_{\omega \gg 0} \chi_{\rho\rho}(\vec{q}, \omega) = -q_e^2 N_s \left(\frac{\omega^{(1)}(\vec{q})}{\omega^2} + \frac{\omega^{(3)}(\vec{q})}{\omega^4} + \dots \right), \quad (\text{F.4})$$

where the frequency moments $\omega^{(2j+1)}(\vec{q})$ are given by

$$\omega^{(2j+1)}(\vec{q}) = \frac{1}{q_e^2 N_s} \int_{-\infty}^{\infty} \frac{d\omega}{\pi} \omega^{2j+1} \chi_{\rho\rho}''(\vec{q}, \omega), \quad (\text{F.5})$$

or upon using Eq. (F.2)

$$\omega^{(2j+1)}(\vec{q}) = \frac{2}{q_e^2 N_s} \int_{-\infty}^{\infty} d\omega \omega^{2j+1} S(\vec{q}, \omega). \quad (\text{F.6})$$

F.2 High frequency moments: irreducible susceptibility

In the presence of long-ranged Coulomb interactions it is necessary [5] to distinguish between reducible susceptibility (or polarization) $\chi_{\rho\rho}$ and the irreducible susceptibility (or polarization) $\tilde{\chi}_{\rho\rho}$. The irreducible susceptibility $\tilde{\chi}_{\rho\rho}$ can be shown to satisfy a spectral representation

$$\tilde{\chi}_{\rho\rho}(\vec{q}, \omega) = -\frac{1}{\pi} \int_{-\infty}^{\infty} d\nu \frac{\tilde{\chi}_{\rho\rho}''(\vec{q}, \nu)}{\omega - \nu + i0^+}. \quad (\text{F.7})$$

This is completely analogous to Eq. (F.3), and using a moment expansion analogous to Eq. (F.4) we get

$$\lim_{\omega \gg 0} \tilde{\chi}_{\rho\rho}(\vec{q}, \omega) = -q_e^2 N_s \left(\frac{\tilde{\omega}^{(1)}(\vec{q})}{\omega^2} + \frac{\tilde{\omega}^{(3)}(\vec{q})}{\omega^4} + \dots \right), \quad (\text{F.8})$$

In order to determine the moments $\tilde{\omega}^{(2l+1)}(\vec{q})$, we recast Eq. (31) in the form

$$\tilde{\chi}_{\rho\rho}(\vec{q}, \omega) = \frac{\chi_{\rho\rho}(\vec{q}, \omega)}{1 - \frac{V(\vec{q})}{N_s} \chi_{\rho\rho}(\vec{q}, \omega)}. \quad (\text{F.9})$$

We next plug into this expression the high frequency expansion Eq. (F.4) giving an infinite series in $\frac{1}{\omega^2}$. Comparing with Eq. (F.8), the moments $\tilde{\omega}^{(2j+1)}(\vec{q})$ can be determined in terms of $\omega^{(2j+1)}(\vec{q})$. For our purpose we only need the first moment:

$$\tilde{\omega}^{(1)}(\vec{q}) = \omega^{(1)}(\vec{q}). \quad (\text{F.10})$$

We make extensive use of the first moment $\omega^{(1)}(\vec{q})$ below, let us note that it is in frequency units and provides a very important scale in the problem. We now relate this frequency to $\kappa(\vec{q})$. From Eq. (32) we note that

$$\lim_{\omega \gg 0} \varepsilon(\vec{q}, \omega) \rightarrow 1 - V(\vec{q}) N_s \left(\frac{\tilde{\omega}^{(1)}(\vec{q})}{\omega^2} + \frac{\tilde{\omega}^{(3)}(\vec{q})}{\omega^4} + \dots \right). \quad (\text{F.11})$$

Comparing the leading term with the expression in Eq. (E.6, E.7), we get

$$\tilde{\omega}^{(1)}(\vec{q}) = \frac{a_0 \hbar}{q_e^2} \kappa(\vec{q}), \quad (\text{F.12})$$

where we temporarily reintroduced the lattice constant a_0 and \hbar to emphasize that $\tilde{\omega}^{(1)}$ is in frequency units, while κ is the square of a frequency [38].

Using Eq. (E.7), the first moment also determines the plasmon energy as $\omega_p(\vec{q}) = \sqrt{\frac{N_s}{q_e^2} V(\vec{q}) \kappa(\vec{q})}$. Proceeding further we can express $\kappa(\vec{q})$ in 2-d explicitly in terms of \vec{q} , the band hopping parameters and the averages over the momentum distribution function $\langle \tilde{C}_k^\dagger \tilde{C}_k \rangle$ of the type $\langle \cos k_x \rangle_{ave} \equiv \frac{1}{N_s} \sum_k \cos k_x \langle \tilde{C}_k^\dagger \tilde{C}_k \rangle$. Using Eq. (19) and the band dispersion parameters t, t' representing the nearest and next nearest neighbor hops on the square lattice:

$$\varepsilon_k = -2t(\cos k_x + \cos k_y) - 4t' \cos k_x \cos k_y. \quad (\text{F.13})$$

We find

$$\tilde{\omega}^{(1)}(\vec{q}) = 8t \langle \cos k_x \rangle_{ave} (2 - \cos q_x - \cos q_y) + 16t' \langle \cos k_x \cos k_y \rangle_{ave} (1 - \cos q_x \cos q_y). \quad (\text{F.14})$$

For small \vec{q} we find

$$\lim_{\vec{q} \rightarrow 0} \tilde{\omega}^{(1)}(\vec{q}) \rightarrow |\vec{q}|^2 \frac{\mathcal{T}}{q_e^2}, \quad (\text{F.15})$$

where we utilized Eq. (20), and

$$\mathcal{T} = q_e^2 (4t \langle \cos k_x \rangle_{ave} + 8t' \langle \cos k_x \cos k_y \rangle_{ave}) \quad (\text{F.16})$$

We see from Eq. (22) that \mathcal{T} determines the total weight of the optical conductivity. The relevant averages of the cosines are tabulated in Table (1), where we see the enormous reduction from uncorrelated values brought about by the strong correlations.

For completeness we note that our notation for the reducible $\chi_{\rho\rho}$ and irreducible $\tilde{\chi}_{\rho\rho}$ polarizations can be mapped into that used in [13–15] by setting

$$\begin{aligned} \chi_{\rho\rho} &\rightarrow -\chi \\ \tilde{\chi}_{\rho\rho} &\rightarrow -\Pi \\ \varepsilon &\rightarrow \varepsilon/\varepsilon_\infty. \end{aligned} \quad (\text{F.17})$$

References

- [1] T. M. Rice and W. F. Brinkman, “Some aspects of the theory of the Mott transition”, in *Critical Phenomena in Alloys, Magnets and Superconductors*, ed. R. E. Mills, E. Ascher and R. H. Jaffee, p593 (McGraw-Hill, New York) (1971).
- [2] W. F. Brinkman and T. M. Rice, Phys. Rev. B **2**, 4302 (1970).
- [3] D. Vollhardt, Rev. Mod. Phys. **56**, 99 (1984) (esp. Sec. IV).
- [4] We denote by U and t the standard interaction and hopping parameters of the Hubbard model with N_s sites. Here the lattice constant is a_0 , and we denote by q_e the electron charge, i.e. $q_e = -|e|$.
- [5] P. Nozières, in *Theory of Interacting Fermi Systems*, (W. A. Benjamin, New York, 1964).
- [6] A. A. Abrikosov, L. Gor’kov and I. Dzyaloshinski, *Methods of Quantum Field Theory in Statistical Physics*, Prentice-Hall, Englewood Cliffs, NJ (1963).
- [7] A. L. Fetter and J. D. Walecka, *Quantum Theory of Many-Particle Systems*, (McGraw-Hill, New York, 1971.)
- [8] L. P. Kadanoff, G. Baym, *Quantum Statistical Mechanics: Green’s Function Methods in Equilibrium and Nonequilibrium Problems*, Benjamin, NY, 1962.
- [9] Y. Nambu, Phys. Rev. **117**, 648 (1960).
- [10] A. K. Rajagopal, Nucl. Phys. 57, 435 (1964); A. K. Rajagopal, H. Brooks, and N. Ranganathan, Nuovo Cimento, Suppl. 5, 807 (1967).
- [11] F. Aryasetiawan, M. Imada, A. Georges, G. Kotliar, S. Biermann, and A. I. Lichtenstein, Phys. Rev. B **70**, 195104 (2004).
- [12] M. Casula, Ph. Werner, L. Vaugier, F. Aryasetiawan, T. Miyake, A. J. Millis, and S. Biermann, Phys. Rev. Letts. **109**, 126408 (2012).
- [13] S. Vig, A. Kogar, M. Mitran, A. A. Husain, L. Venema, M. S. Rak, V. Mishra, P. D. Johnson, G. D. Gu, E. Fradkin, M. R. Norman and P. Abbamonte, SciPost Phys. **3**, 026 (2017).

- [14] M. Mitranova, A. A. Husaina, S. Viga, A. Kogara, M. S. Rak, S. I. Rubeck, J. Schmalian, B. Uchoa, J. Schneeloch, R. Zhong, G. D. Gu, and P. Abbamonte, PNAS, **115**, 5392 (2018)
- [15] A. A. Husain, M. Mitrano, M. S. Rak, S. Rubeck, B. Uchoa, K. March, C. Dwyer, J. Scheenloch, R. Zhang, G. D. Gu and P. Abbamonte, Phys. Rev. X **9**, 041062 (2019)
- [16] C. M. Varma, P. B. Littlewood, S. Schmitt-Rink, E. Abrahams and A. E. Ruckenstein, Phys. Rev. Letts. **63**, 1999 (1989).
- [17] C. M. Varma, Phys. Rev. B **96**, 075122 (2017).
- [18] B. S. Shastry, Phys. Rev. Letts. **107**, 056403 (2011); Ann. Phys. **343**, 164-199 (2014). <http://physics.ucsc.edu/~sriram/papers/ECFL-Reprint-Collection.pdf>
- [19] B. S. Shastry, Phys. Rev. B **81**, 045121 (2010).
- [20] M. Arciniaga, P. Mai and B. S. Shastry, Phys. Rev. B **101**, 245149 (2020)
- [21] P. Mai and B. S. Shastry, Phys. Rev. B **98**, 205106 (2018); B. S. Shastry and P. Mai, New Jour. Phys. **20** 013027 (2018).
- [22] F. Stern, Phys. Rev. Letts. **18**, 546 (1967).
- [23] S. Das Sarma, S. Adam, E. H. Hwang, and Enrico Rossi, Rev.Mod. Phys. **83**, 407 (2011).
- [24] E. H. Hwang and S. Das Sarma, Phys. Rev. B **75**, 205418 (2007).
- [25] H.L.Störmer, R.Dingle, A.C.Gossard, W.Wiegmann, M.D.Sturge, Sol. State Comm **29**, 705 (1979).
- [26] J. M. Luttinger, Phys. Rev. **121**, 942 (1960); esp. Sec. 2.
- [27] B. S. Shastry, [arXiv:1104.2633](https://arxiv.org/abs/1104.2633); Phys. Rev. B **84**, 165112 (2011); Phys. Rev. B **86**, 079911(E) (2012).
- [28] H. Mori, Prog. Theor. Phys. **33**, 423 (1965); **34**, 399 (1965).
- [29] M. Dupuis, Prog. Theor. Phys. **37**, 502 (1967)
- [30] Peizhi Mai and B. Sriram Shastry, Phys. Rev. B. **98**, 115101, (2018).
- [31] B. S. Shastry and P. Mai, Phys. Rev. B **101**, 115121 (2020).
- [32] B S Shastry, Phys. Rev. B **73**, 085117 (2006).
- [33] G.-H. Gweon, B. S. Shastry and G. D. Gu, Phys. Rev. Letts. **107**, 056404 (2011).
- [34] M. M. Qazilbash, A. Koitzsch, B. S. Dennis, A. Gozar, H. Balci, C. A. Kendziora, R. L. Greene, and G. Blumberg, Phys. Rev. B **72**, 214510 (2005); A. Koitzsch, G. Blumberg, A. Gozar, B. S. Dennis, P. Fournier, and R. L. Greene, Phys. Rev. B **67**, 184522 (2003).
- [35] S. Sugai, J. Nohara, R. Shiozaki, T. Muroi, Y. Takayanagi, N. Hayamizu, K. Takenaka, and K. Okazaki, J. Phys.: Condens. Matter **25**, 415701 (2013); S. Sugai, Y. Takayanagi, N. Hayamizu, T. Muroi, J. Nohara, R. Shiozaki, K. Okazaki, and K. Takenaka, Physica C **470**, S97 (2010).
- [36] J. Hubbard, Proc. Phys. Soc., London, Sect. A **68**, 976 (1955); K. S. Singwi, M. P. Tosi, R. H. Land, and A. Sjolander Phys. Rev. **176**, 589 (1968); A. Holas, S. Rahman, Phys. Rev. B **35**, 2720 (1987);
- [37] B S Shastry, Rep. Prog. Phys. **72** 016501 (2009); Eq. (6) and Eq. (64).
- [38] A comment on the dimensions of these variables may be useful. The variables $\kappa(\vec{q})$ and \mathcal{T} have dimensions of frequency squared. This feature is submerged in the notation since we have set the lattice constant $a_0 \rightarrow 1$ and also set $\hbar \rightarrow 1$. To restore the dimensions we should read Eq. (19) as

$$\kappa(\vec{q}) = \frac{2q_e^2}{a_0 \hbar^2 N_s} \sum_{k\sigma} \left(\varepsilon_{\vec{k}+\vec{q}} - \varepsilon_{\vec{k}} \right) \langle \tilde{C}_{\vec{k}\sigma}^\dagger \tilde{C}_{\vec{k}\sigma} \rangle. \quad (\text{F.18})$$

and Eq. (21) as

$$\mathcal{T} = \frac{q_e^2}{a_0 N_s \hbar^2} \sum_{k\sigma} \left(\frac{d^2 \varepsilon_{\vec{k}}}{d(k_x a_0)^2} \right) \langle \tilde{C}_{\vec{k}\sigma}^\dagger \tilde{C}_{\vec{k}\sigma} \rangle, \quad (\text{F.19})$$

- [39] D. L. Mills, Surf. Sci. **48**, 59 (1975).
- [40] D. N. Basov and T. Timusk, Rev. Mod. Phys. **77**, 721 (2005); J Orenstein, G A Thomas, A J Millis, S L Cooper, D H Rapkine, T Timusk, L F Schneemeyer, J V Waszczak, Phys. Rev. B **42**, 6342 (1990); D. van der Marel, F. Carbone, A. B. Kuzmenka and F. Giannini, Ann. Phys. **321**, 1716 (2006).

- [41] K. N. Pathak and P. Vashishta, Phys. Rev. B **7**, 3649 (1973).
- [42] This is also true theoretically, as seen in Fig. (17, 19). (We checked the continuity in \vec{q} by independent calculations of the two sets of variables using the current vertex defined by Eq (2) of [30].
- [43] For this purpose it may be more useful to rewrite Eq. (80) in the form

$$\Omega_p^2(\vec{q}) = \frac{\int_{-\infty}^{\infty} d\omega \, \omega \, \text{Im} \, \widetilde{\chi}_{\rho\rho}(\vec{q}, \omega)}{\int_{-\infty}^{\infty} d\omega \, \frac{1}{\omega} \, \text{Im} \, \widetilde{\chi}_{\rho\rho}(\vec{q}, \omega)}. \quad (\text{F.20})$$

For the purpose of estimation, one may perform both integrations over the finite range of available frequencies. The estimate can be quite reasonable if the range is not too small.

- [44] J. Town et al., “XSEDE: Accelerating Scientific Discovery”, Computing in Science & Engineering, Vol.16, No. 5, pp. 62-74, Sept.-Oct. 2014, doi:10.1109/MCSE.2014.80

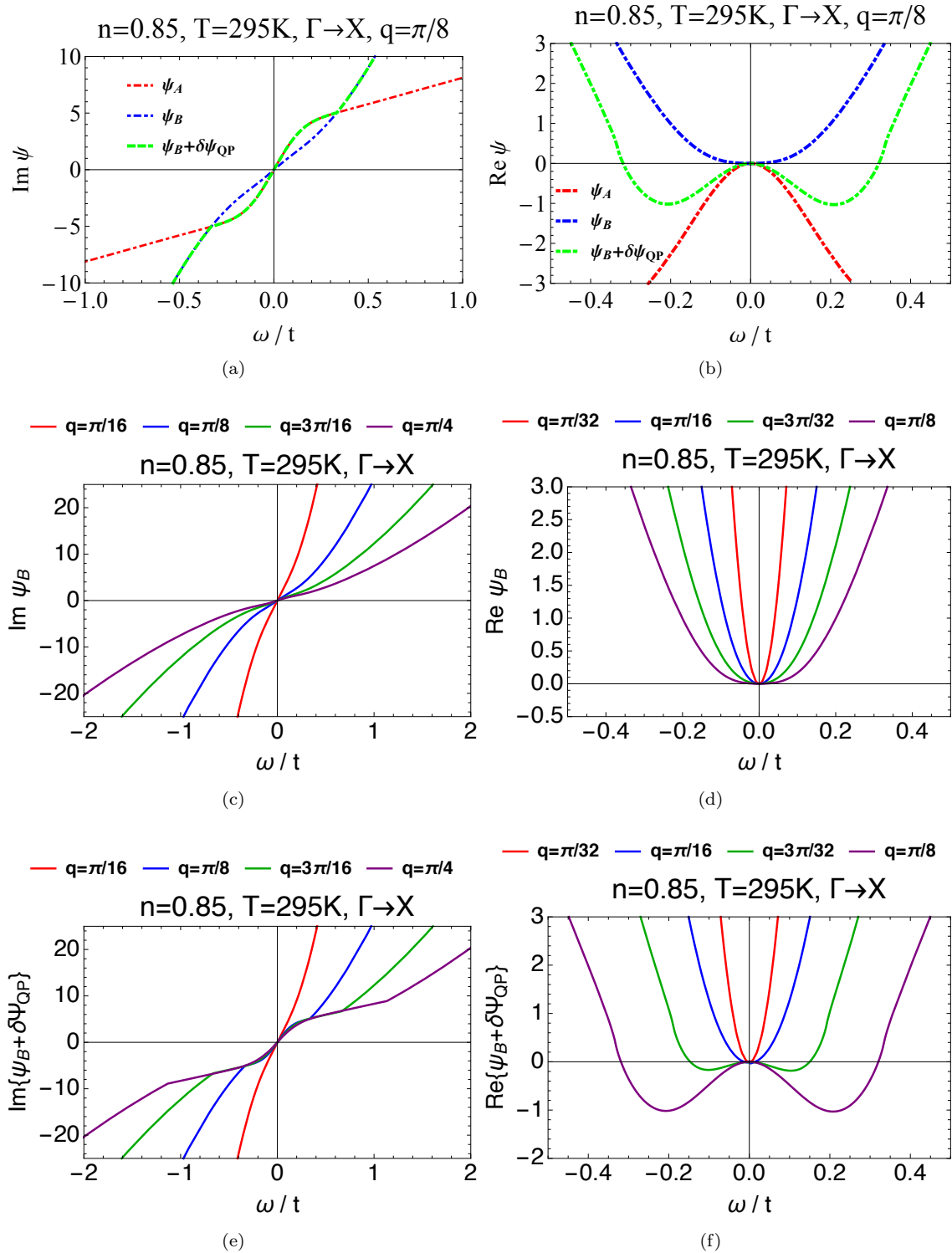


Figure 7: The complex self energy $\Psi(\vec{q}, \omega)$ of the susceptibility $\tilde{\chi}_{\rho\rho}(\vec{q}, \omega)$ as defined in Eq. (50). We show Ψ_A and Ψ_B given in Eq. (66, 67, 71, 72) at density $n = 0.85$ and $T = 297\text{K}$ along the $\Gamma \rightarrow X$ direction where $\vec{q} = (q, q)$. Panels (a) and (b) show the effects of adding the quasiparticle contribution $\delta\Psi_{QP}$ to Ψ_B in the imaginary and real parts of the self energy. Panels (c) and (d) show the imaginary and real parts of $\Psi_B(\vec{q}, \omega)$ and panels (e) and (f) shows the imaginary and real parts of $\Psi_B(\vec{q}, \omega) + \delta\Psi_{QP}(\vec{q}, \omega)$ for a few q values.

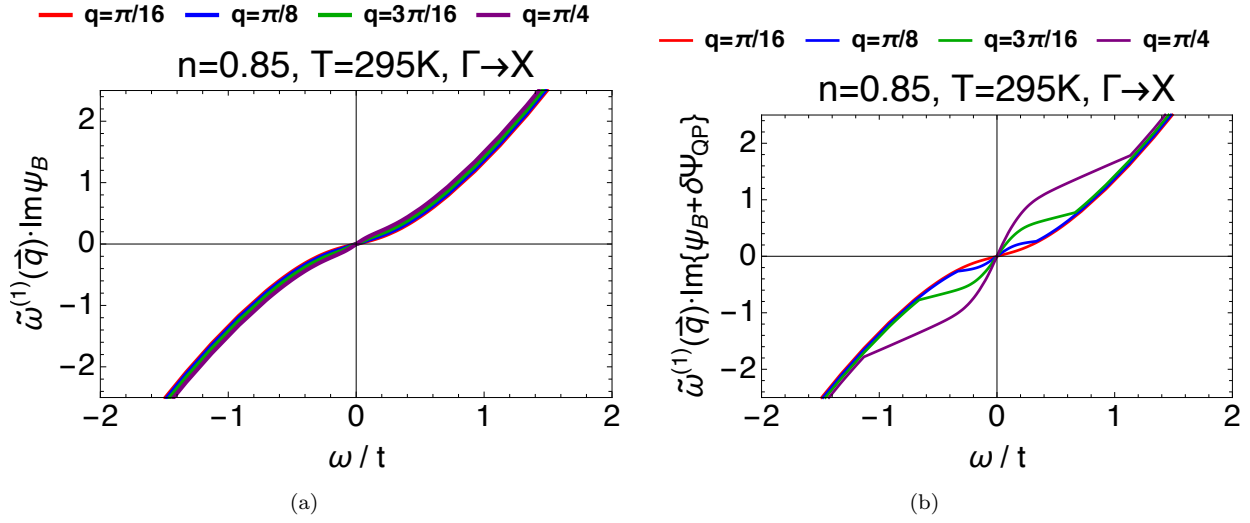


Figure 8: (a) The imaginary part of the self energy $\Psi_B(\vec{q}, \omega)$ (Eq. (67)) at different values of $\vec{q} = (q, q)$ (in $\Gamma \rightarrow X$ direction) coincide and collapse to a single curve when scaled by the first moment $\tilde{\omega}^{(1)}(\vec{q})$ (Eq. (F.4)). (b) For $\Psi_B(\vec{q}, \omega) + \delta\Psi_{QP}(\vec{q}, \omega)$ the imaginary part of the self-energy also coincide, but only at high frequencies beyond the energy scale of the quasiparticle excitations. From Eq. (60) we see that the (on-shell) product $\tilde{\omega}^{(1)}(\vec{q}) \text{Im} \Psi(\vec{q}, \Omega_p(\vec{q}))$ equals the squared width $\Gamma_p^2(\vec{q})$ of the peak in $\text{Im} \tilde{\chi}_{\rho\rho}(\vec{q}, \omega)$, located at $\omega \sim \Omega_p(\vec{q})$. On the other hand the (off-shell) case Eq. (56) for generic ω describes the almost \vec{q} independent fall off away from the peak.

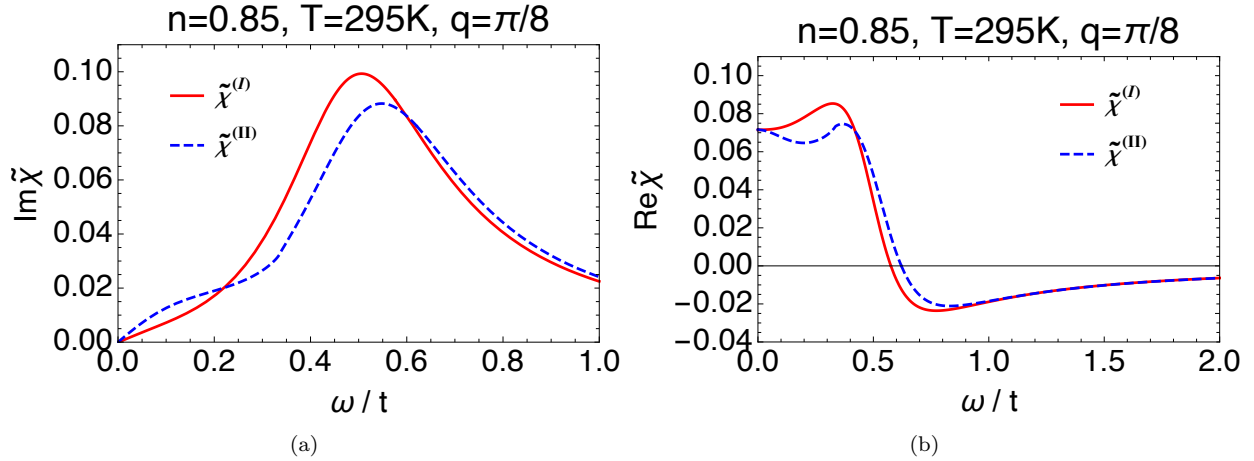


Figure 9: A comparison between the (a) imaginary and (b) real parts of the susceptibilities $\tilde{\chi}^{(I)}$ and $\tilde{\chi}^{(II)}$ from Eq. (69) and Eq. (70). The quasiparticle contribution is visible in (a) at low frequencies, and is roughly linear in ω .

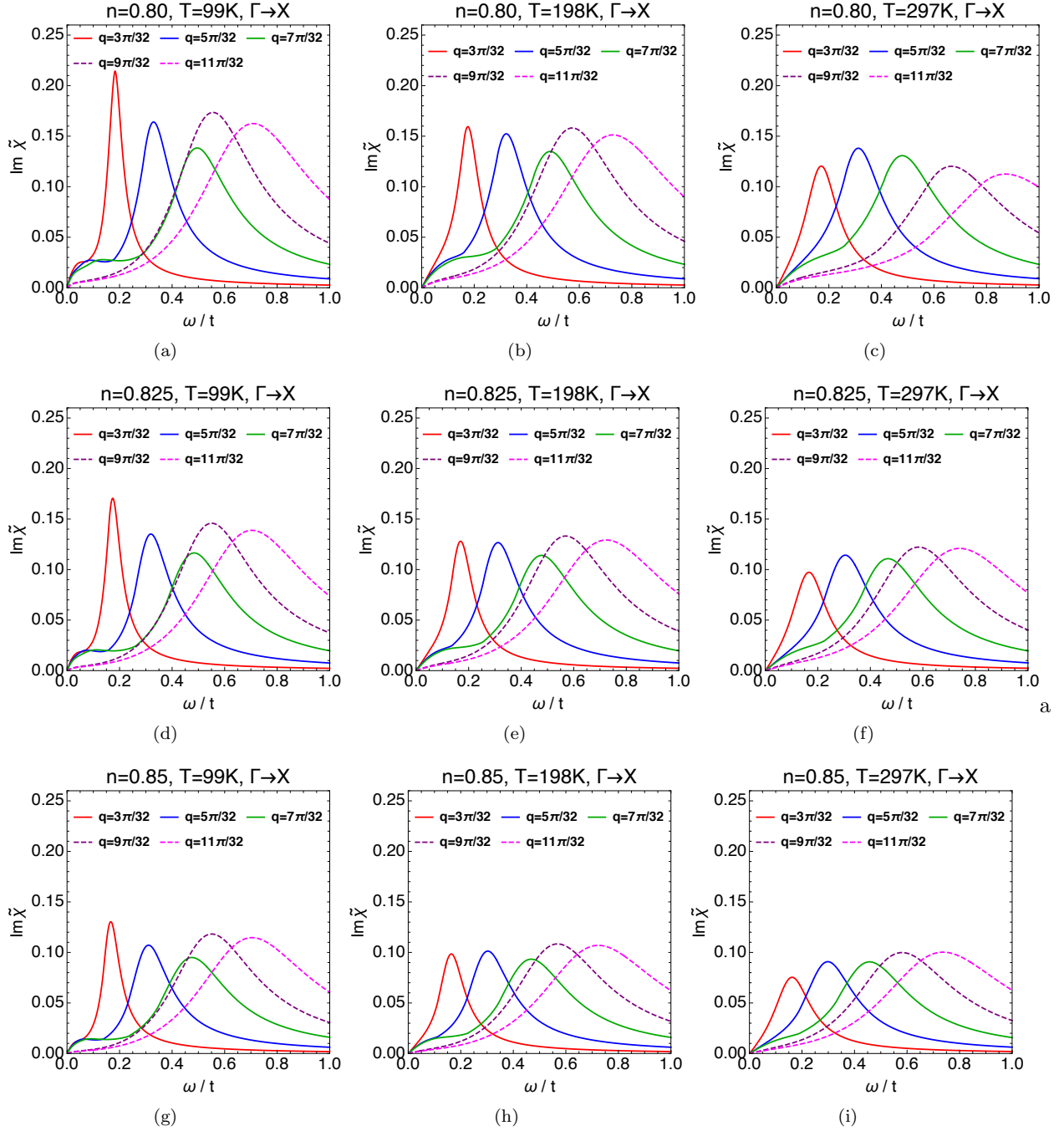


Figure 10: The two susceptibilities $\text{Im } \tilde{\chi}^{(I)}$ Eq. (69) (dashed) and $\text{Im } \tilde{\chi}^{(II)}$ Eq. (70) (solid) at densities $n = 0.8, 0.825, 0.85$ at temperatures $T = 99, 198, 297\text{K}$ in the $\Gamma \rightarrow X$ direction where $\vec{q} = (q, q)$. These curves exhibit a \vec{q} dependent peak at $\Omega_p(\vec{q}) \sim \Omega(\vec{q}, 0)$ from Eq. (59), detailed in Fig. (12).

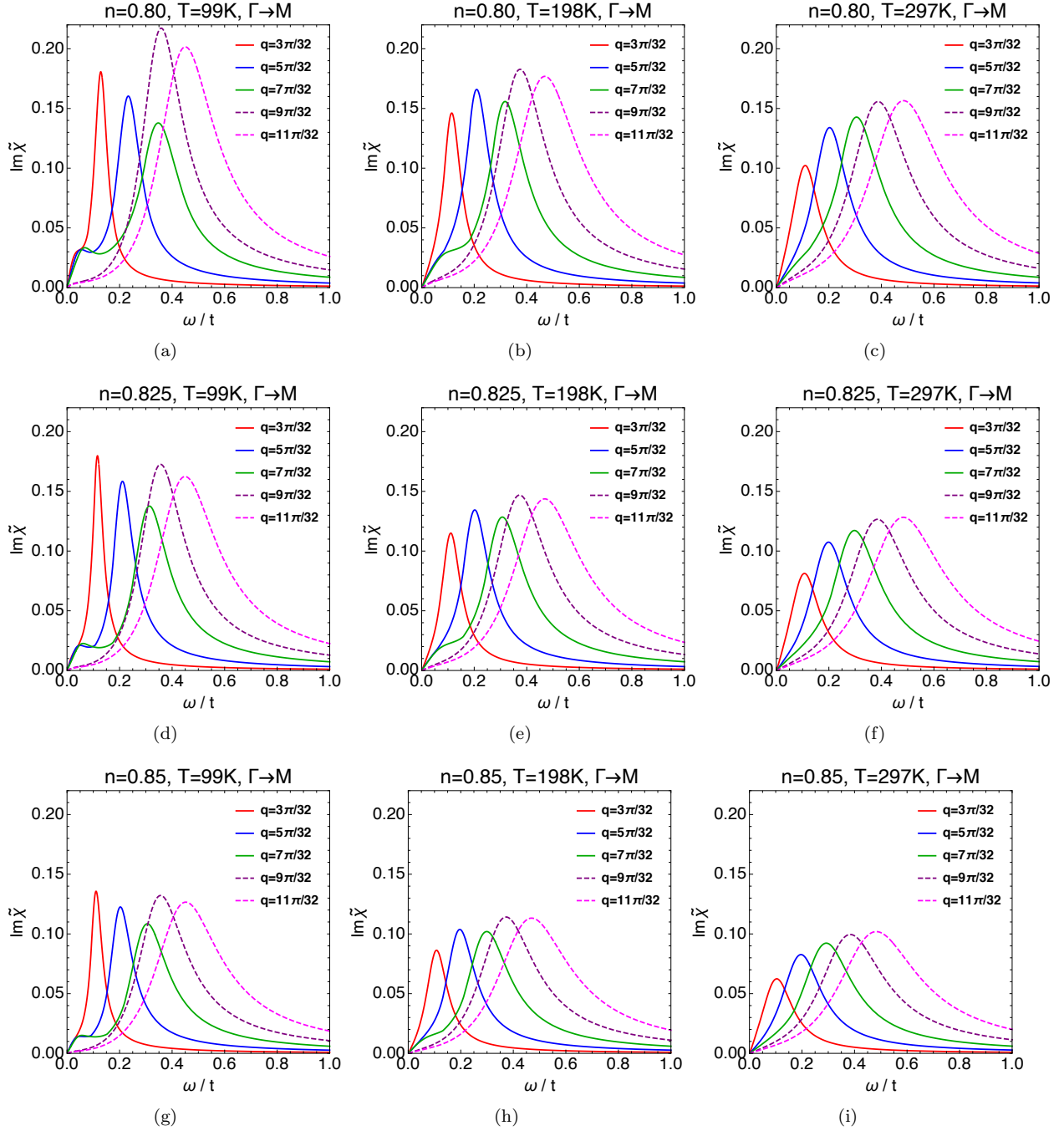


Figure 11: The same two susceptibilities as Fig. (10): $\text{Im } \tilde{\chi}^{(I)}$ Eq. (69) (dashed) and $\text{Im } \tilde{\chi}^{(II)}$ Eq. (70) (solid) at densities $n = 0.8, 0.825, 0.85$ at temperatures $T = 99, 198, 297\text{K}$ in the $\Gamma \rightarrow M$ direction where $\vec{q} = (q, 0)$.

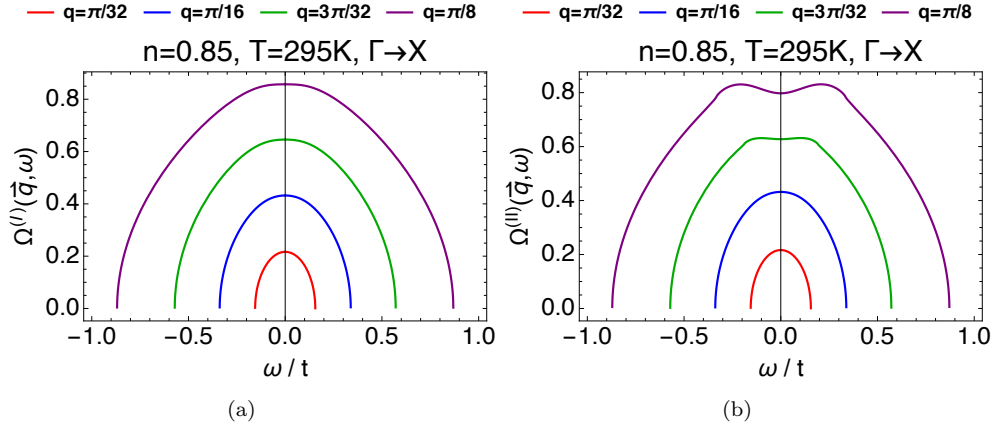


Figure 12: The characteristic energy scale Eq. (57) in units of t . In panel (a) $\Omega^{(I)}$ uses Eq. (69), and panel (b) $\Omega^{(II)}$ uses Eq. (70), leading to similar energies. Here $n = 0.85$ and $T = 297\text{K}$ and $\vec{q} = (q, q)$. The peaks in $\text{Im} \tilde{\chi}_{\rho\rho}(\vec{q}, \omega)$ are located at the roots of $\omega^2 = \Omega^2(\vec{q}, \omega)$ Eq. (56), or approximately at the peak energy $\Omega_p(\vec{q}) \sim \Omega(\vec{q}, 0)$. It therefore represents the peak energy scale observed in Fig. (10, 11, 17, 18, 19).

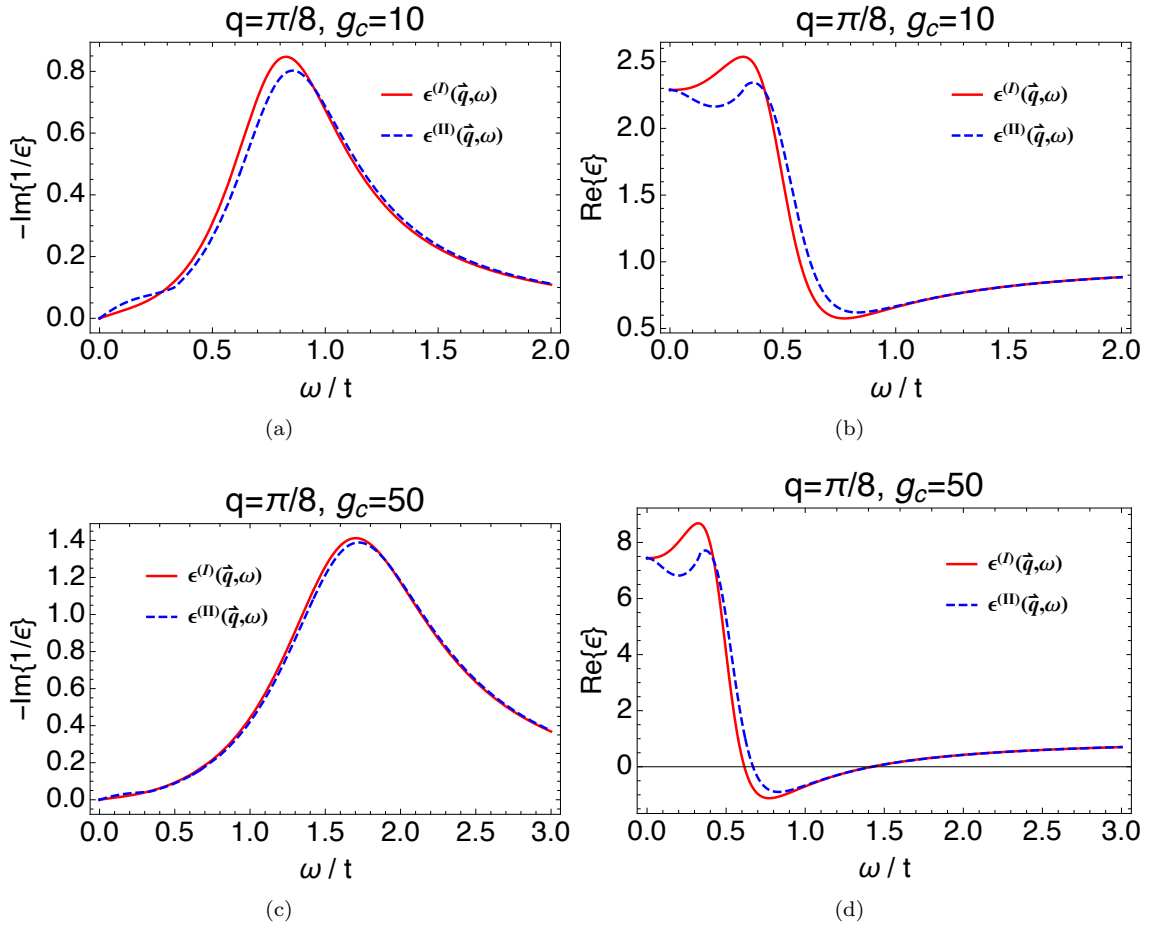


Figure 13: The dielectric constants $\epsilon^{(I)}$ and $\epsilon^{(II)}$ from Eq. (73) for a system at $n = 0.85$ and $T = 297\text{K}$, with $\vec{q} = (q, q)$ along $\Gamma \rightarrow X$. Here panel (a), (c) is the imaginary part while panel (b), (d) is the real part for $g_c = 10, 50$ respectively. The curves $\text{Re} \epsilon^{(I, II)}$ do not vanish in this range at $g_c = 10$ (panel(b)), while they do so when $g_c = 50$ (panel(d)). This is unlike plasmon in weakly interacting electron gas discussed in books Ref. [7], where a zero crossing accurately determines the plasmon.

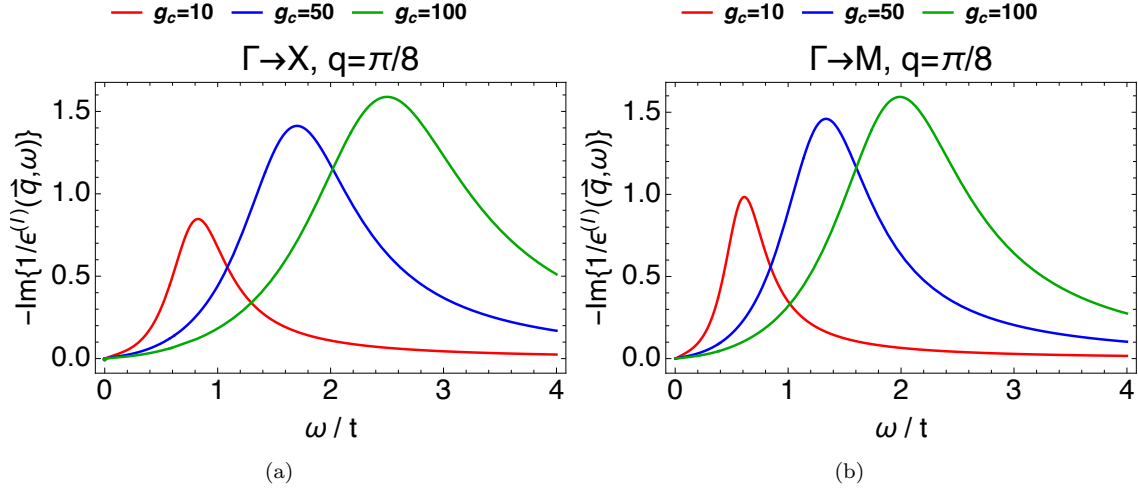


Figure 14: Imaginary part of inverse dielectric function (Eq. (73)) at $n = 0.85$ and $T = 297\text{K}$. Panels (a) $\vec{q} = (\pi/8, \pi/8)$ and (b) $\vec{q} = (\pi/8, 0)$ illustrate the variation of the plasmon peak with g_c in the respective directions.

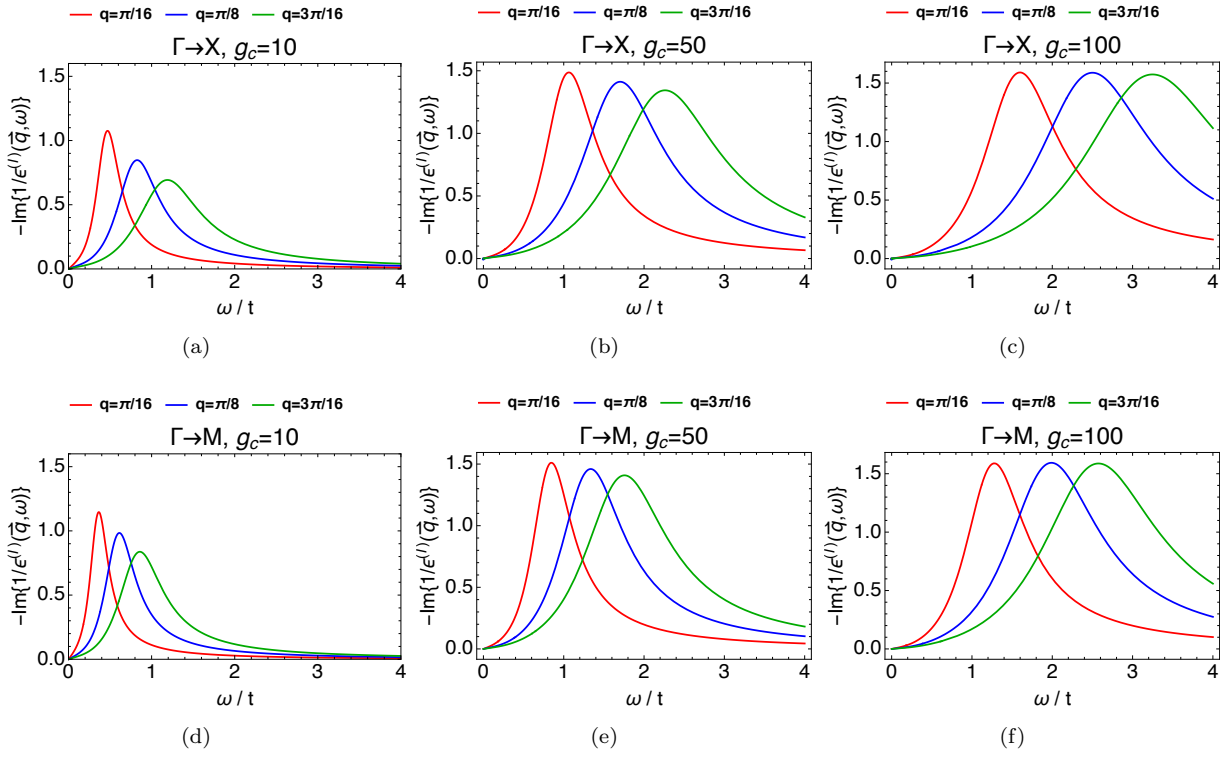


Figure 15: Imaginary part of inverse dielectric function (Eq. (73)) at $n = 0.85$ and $T = 297\text{K}$. Panels (a, b, c) $\Gamma \rightarrow X$ where $\vec{q} = (q, q)$ and (d, e, f) $\Gamma \rightarrow M$ where $\vec{q} = (q, 0)$ exhibit the peak variation with \vec{q} at $g_c = 10, 50, 100$ in the respective directions.

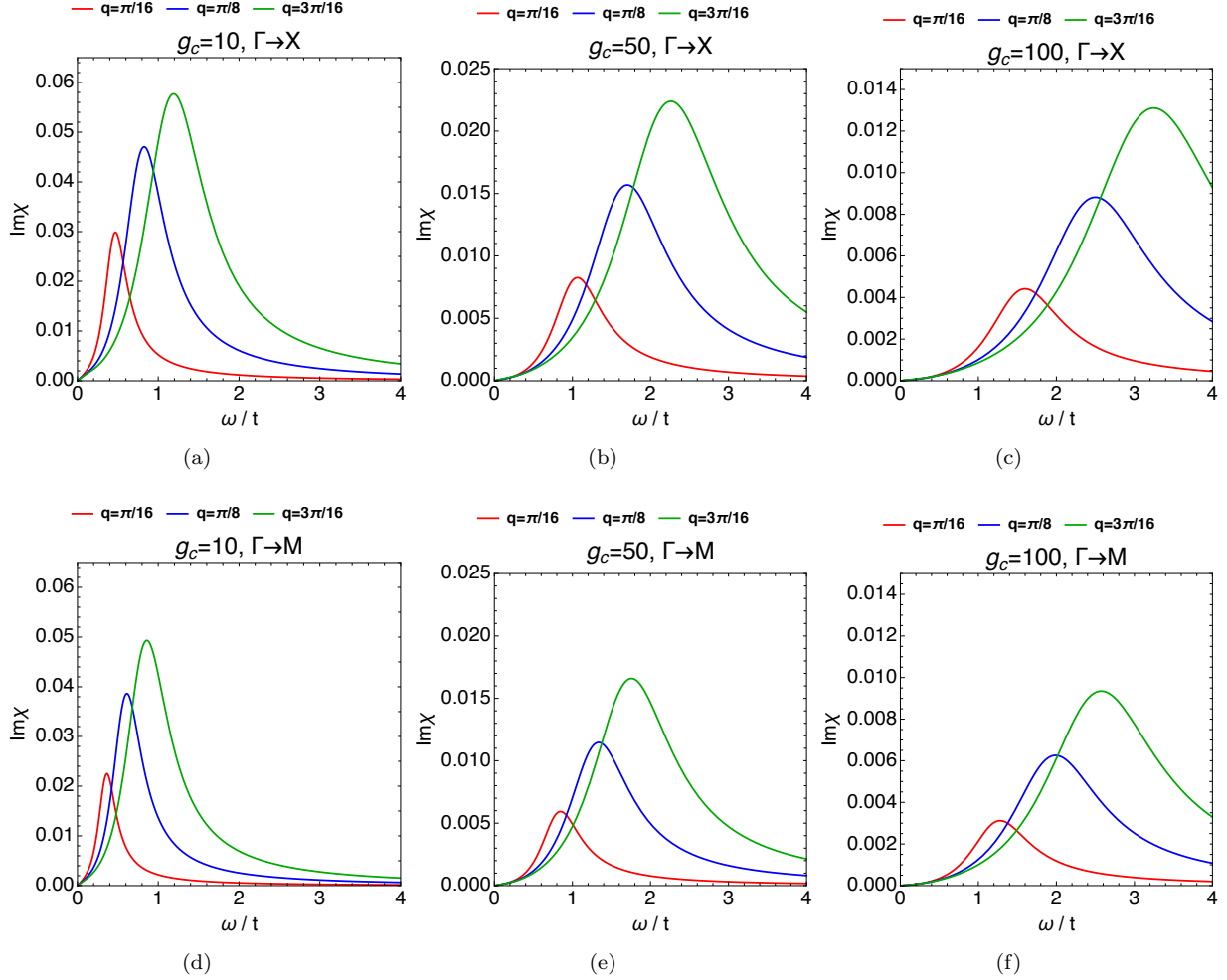


Figure 16: The unscreened susceptibility $\text{Im}\chi_{\rho\rho}$ (Eq. (31)) at $n = 0.85$ and $T = 297\text{K}$. For panels (a, b, c) $\Gamma \rightarrow X$ where $\vec{q} = (q, q)$ and (d, e, f) $\Gamma \rightarrow M$ $\vec{q} = (q, 0)$ exhibit the variation of the plasmon peaks with \vec{q} in their respective directions at the displayed g_c . We used $\tilde{\chi}^{(I)}$ in Eq. (31) here. $\text{Im}\chi_{\rho\rho}$ is the most directly accessible object in inelastic electron scattering experiments Eq. (B.6). In these panels, a decrease in magnitude of the peak as $q \rightarrow 0$ is the consequence of the conservation of charge $\lim_{q \rightarrow 0} \rho q$. We also observe that as g_c increases, the peaks in $\text{Im}\chi_{\rho\rho}$ are broadened and pushed to higher energies.

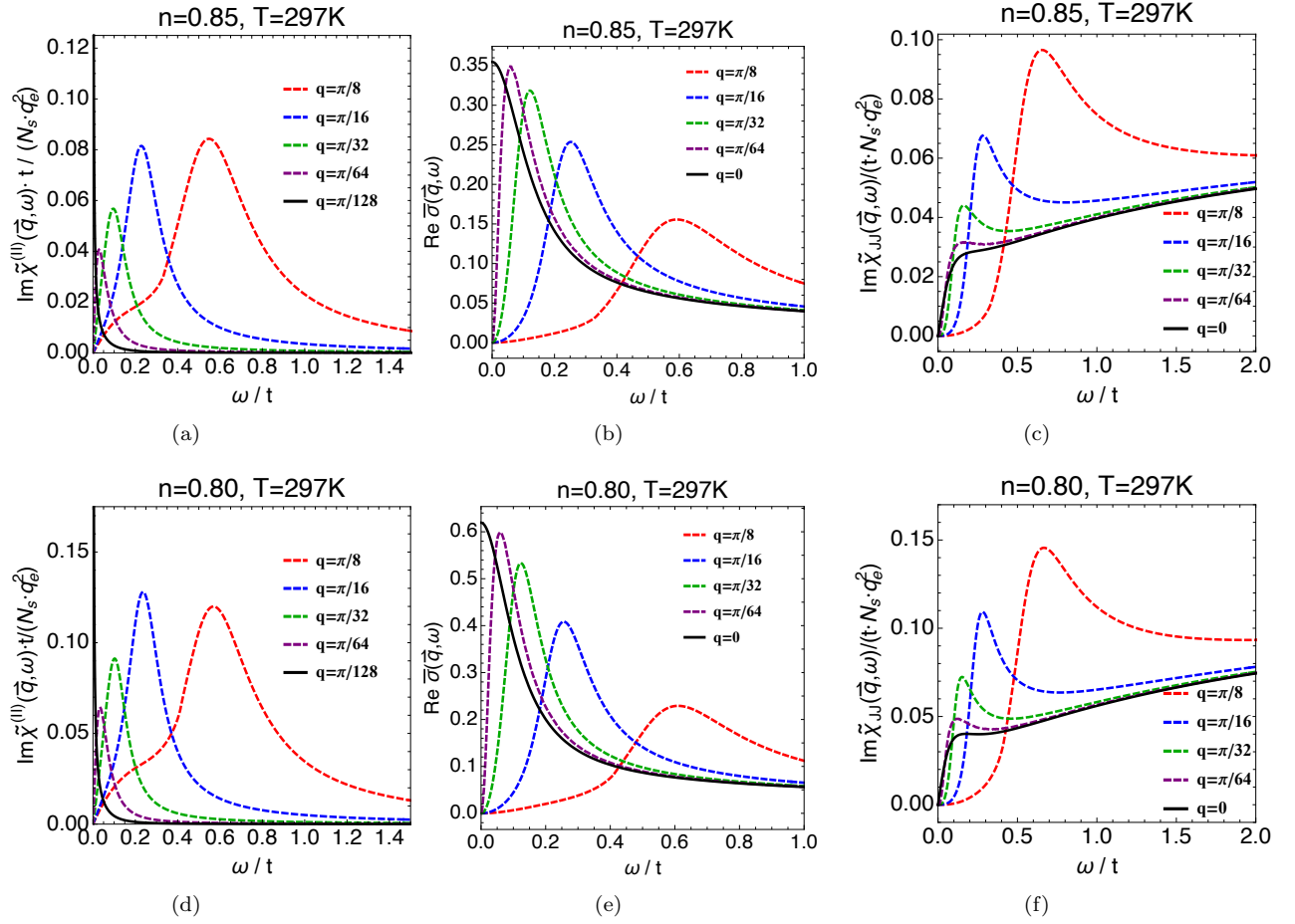


Figure 17: Panels (a,d) display $\text{Im } \tilde{\chi}_{\rho\rho}$, panels (b,e) display $\text{Re } \tilde{\sigma}$ and panels (c,f) $\text{Im } \tilde{\chi}_{JJ}$ with the displayed prefactors. Here $T = 297\text{K}$ and the density is as shown and $\vec{q} = (q, q)$ is along $\Gamma \rightarrow X$. This computation used $L_x \times L_y = 128 \times 128$. The real part of the conductivity $\sigma(\vec{q}, \omega)$ (Eq. (E.13, E.17)), the imaginary part of current susceptibility $\tilde{\chi}_{JJ}$ (Eq. (E.14, 81)) and imaginary part of density susceptibility $\tilde{\chi}^{(II)}$ (Eq. (70)) are related by Eq. (82). In going from panels (a to c) or from (d to f), apart from other constants the second and third objects are found by multiplying the first and second objects with ω respectively. This multiplication causes the peak frequencies to be slightly different in these objects. The flattening of the curves for $\text{Im } \tilde{\chi}_{JJ}$ for all \vec{q} beyond the peak imply that $\text{Im } \tilde{\chi}_{\rho\rho}$ falls off as $1/\omega^2$ in that region. The peaks of all three variables are roughly at the same frequency. The solid black lines for $\vec{q} = 0$ in panels (c,f) are separately computed using the current vertex as defined by Eq. (2) of Ref. [30]. Reconciling the available optical conductivity data with the finite \vec{q} measurements in the MEELS experiments [13–15] is therefore of considerable interest. Theoretical results for both sets of variables, as in panels (a,b) or in (c,d) are of potential use in such a task.

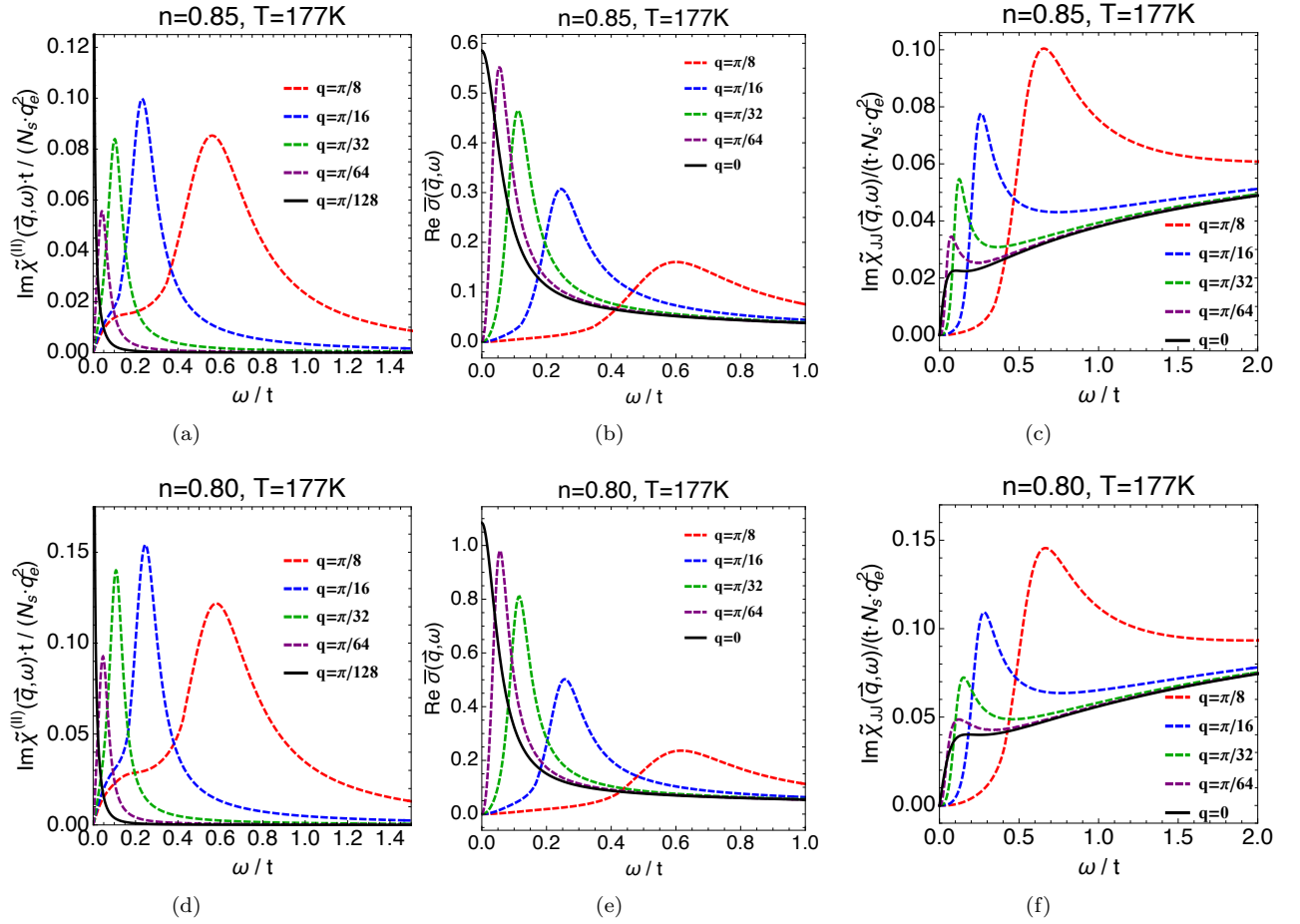


Figure 18: Panels (a,d) display $\text{Im } \tilde{\chi}_{\rho\rho}$, panels (b,e) display $\text{Re } \bar{\sigma}$ and panels (c,f) $\text{Im } \tilde{\chi}_{JJ}$ with the displayed prefactors. Here $T=177\text{K}$ and the density is as shown and $\vec{q} = (q, q)$ is along $\Gamma \rightarrow X$. See the caption of Fig. (17) for further common details.

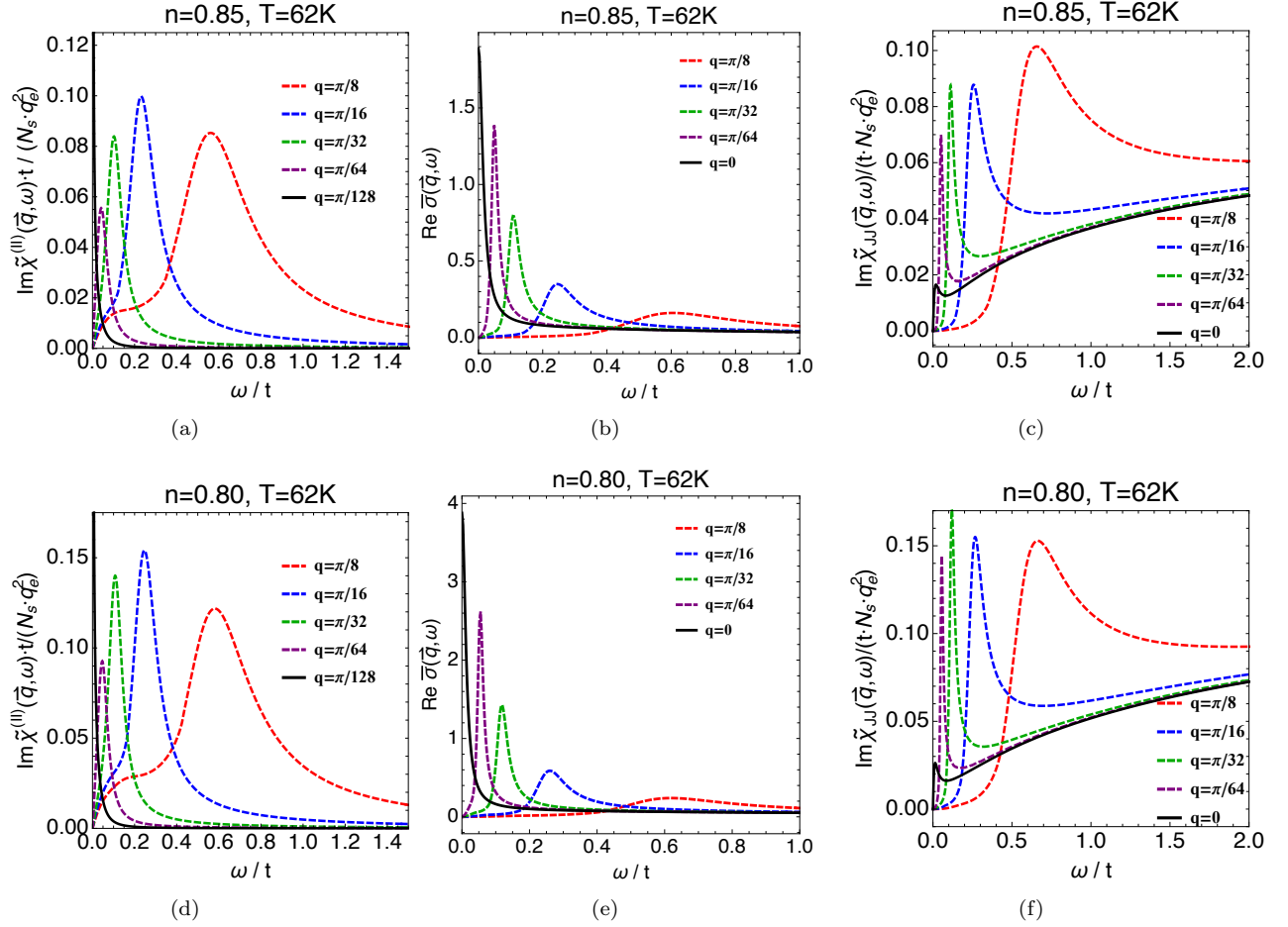


Figure 19: Panels (a,d) display $\text{Im} \tilde{\chi}_{\rho\rho}$, panels (b,e) display $\text{Re} \bar{\sigma}$ and panels (c,f) $\text{Im} \tilde{\chi}_{JJ}$ with the displayed prefactors. Here $T=62\text{K}$ and the density is as shown and $\vec{q} = (q, q)$ is along $\Gamma \rightarrow X$. See the caption of Fig. (17) for further common details.

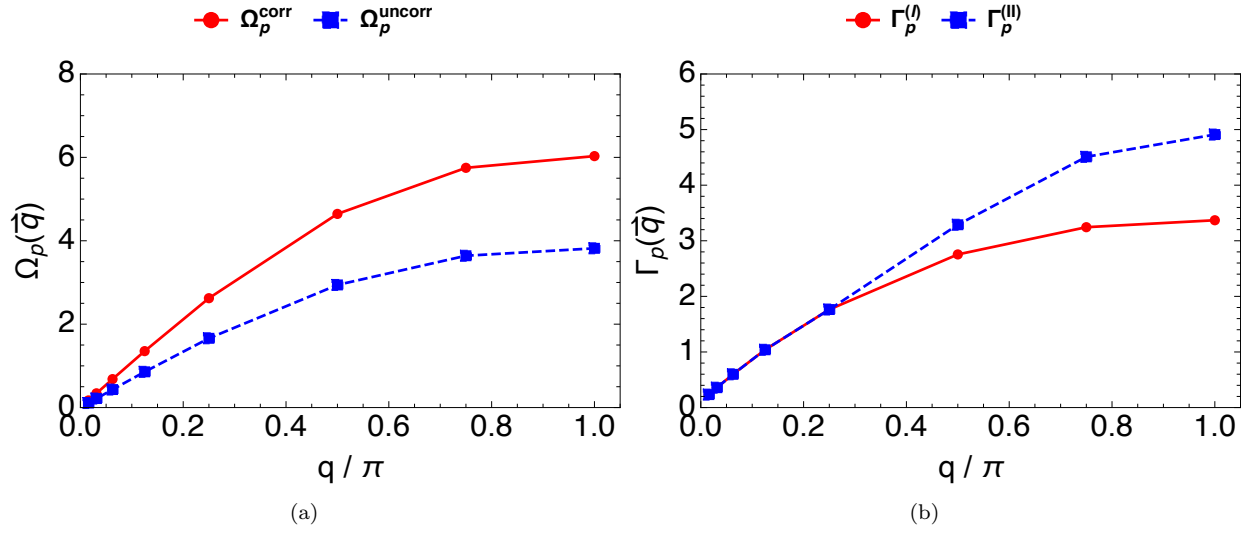


Figure 20: Panel (a) The peak energy scale $\Omega_p(\vec{q})$ (Eq. (59)) and panel (b) the width of the peaks $\Gamma_p(\vec{q})$ (Eq. (60)). In panel (a) the solid red curve $\Omega_p^{\text{corr}}(\vec{q})$ is defined exactly as presented in Eq. (59) and for the blue dashed curve $\Omega_p^{\text{uncorr}}(\vec{q}) \equiv \lim_{\omega \rightarrow 0} \Omega^{(I,II)}(\vec{q}, \omega)$. Note we set $\frac{dn}{d\mu} = \lim_{\vec{q} \rightarrow 0} \tilde{\chi}_{\rho\rho}(\vec{q}, 0)$ for both panels and we note that $\Omega_p^{(I)} = \Omega_p^{(II)}$. In panel (b) the red solid curve $\Gamma_p^{(I)}$ uses $\Psi = \Psi_B$ and the blue dashed curve $\Gamma_p^{(II)}$ uses $\Psi = \Psi_B + \delta\Psi_{QP}$. These computation used $L_x \times L_y = 128 \times 128$. Here $n = 0.85$ and $T = 297\text{K}$ and $\vec{q} = (q, q)$ is along $\Gamma \rightarrow X$.

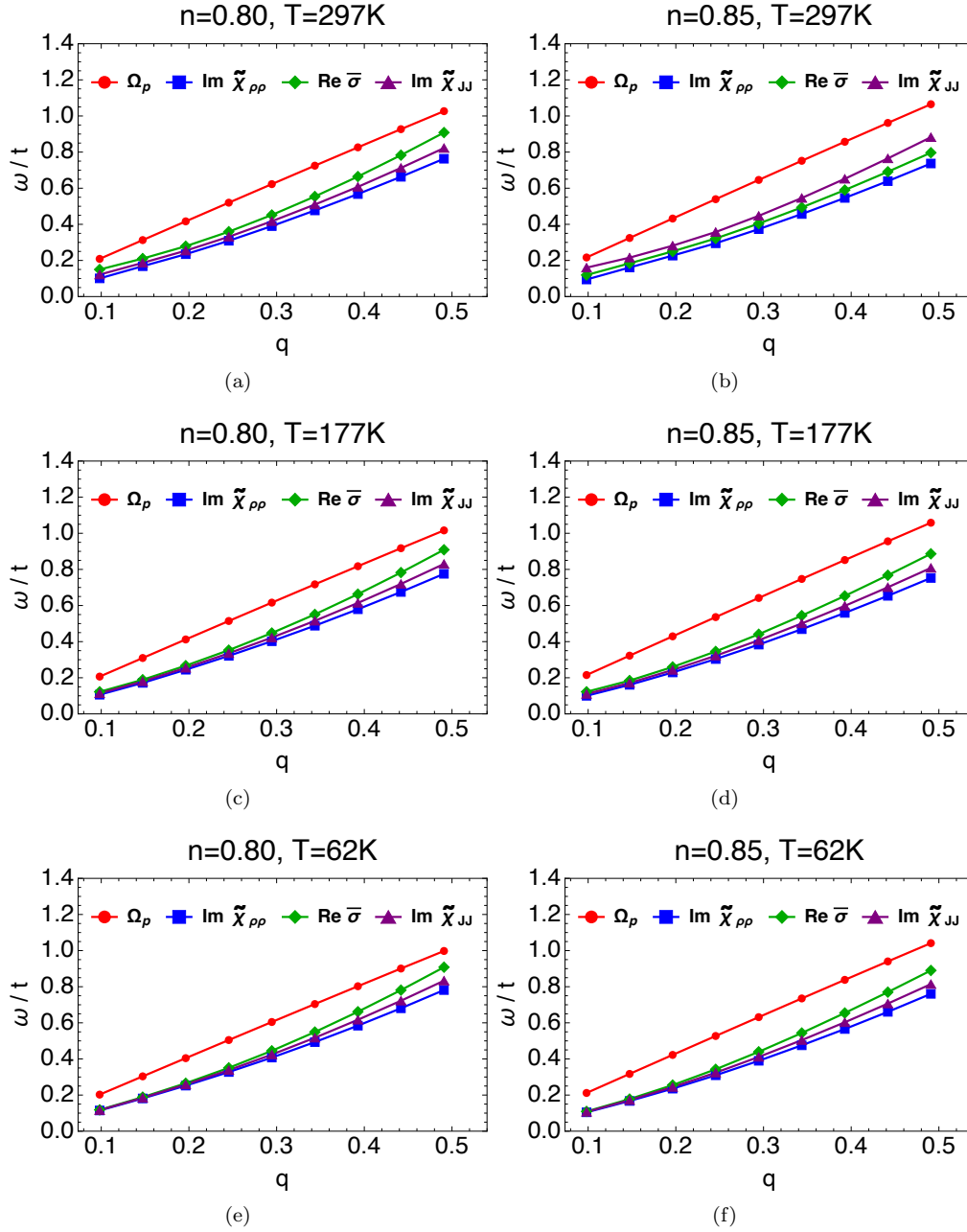


Figure 21: The characteristic frequency scale $\Omega_p(\vec{q})$ (red) Eq. (80) and the turn-around frequency (i.e., peak frequency) for $\text{Im } \tilde{\chi}_{\rho\rho}$ (blue), $\text{Re } \bar{\sigma}$ (green) and $\text{Im } \tilde{\chi}_{JJ}$ (purple) identified from the plots numerically, are compared. This computation used $L_x \times L_y = 128 \times 128$. The screened susceptibility $\tilde{\chi}_{\rho\rho}$ is approximated using $\tilde{\chi}^{(I)}$. Here the density and temperature is as shown and $\vec{q} = (q, q)$ is along $\Gamma \rightarrow X$.